nature human behaviour

Supplementary information

https://doi.org/10.1038/s41562-025-02110-y

Evidence from Tinshemet Cave in Israel suggests behavioural uniformity across *Homo* groups in the Levantine mid-Middle Palaeolithic circa 130,000–80,000 years ago

In the format provided by the authors and unedited

Supplementary Information

Table of content:

S1. Tinshemet Cave setting and geology

Tinshemet Cave, also called Mugharet al-Watwat[1], is located on the east bank of Nahal (wadi) Bet Arif (Wadi Adasiyeh), 95 m above sea level (Extended Data Fig. 1). Bedrock is massive limestone of the Turonian (late Cretaceous) Bina Formation. This formation is the uppermost unit of the Judea Group, which is commonly karstified within south-western Samaria[2]. The overlying caprock is chalk of the Mount Scopus Group. Some chalk patches survive today at the hilltops east and west of the cave. Nahal Bet Arif has entrenched, truncated and exposed the cave following Plio-Pleistocene uplift of the region.

The hillslope has common protruding bedrock karren with terra rossa soil pockets. The local low ridges and hills form the transition from the coastal plain in the west to the Samaria ridge in the east. Structurally the region is within the western flank of the Ramallah anticline, where the sedimentary bedrock layers dip gently westward.

The cave is situated at the southern end of a moderate stepped cliff, some 15m elevation above the wadi bed, and 20 m below the hilltop (Extended Data Fig. 1). The cave is an elongated horizontal passage, sub-divided into three 'chambers' (1-3, beginning from the entrance). The width of the first and second chambers is 3-7 m, and their height 4-5 meters. The third chamber is 15 m long, 8 m wide, and up to 9 m high. Small dead-end passages extend from the last two chambers to the north-west and south-east. Surface denudation has breached the top of the last chamber, forming a small (tens of cm) chimney-like opening to the surface. The last chamber is inhabited today by Egyptian fruit bats (*Rousettus aegyptiacus)* which deposited a guano layer on the floor.

The cave morphology shows elliptical cross sections, smooth walls, and solutional cupolas. The bedrock bottom of the First Chamber, exposed during the present excavation, shows a widened rift-like fracture extending along the passage axis. All these features, combined with the chalk caprock covering the surrounding hills, indicate that the cave formed under hypogenic, confined water circulation[2], commonly forming isolated caves in south-western Samaria[3]. The cave structure seems intermediate between that of chamber caves common to the east, e.g. Rantis Cave, 4 km to the NE[4] and maze-like caves to the west, e.g. Bet Arif Cave, 0.5 km NW of Tinshemet[5].

The bottom of the cave is covered by loose sediments, fruit-bat guano, and fallen bedrock debris. Anthropogenic cemented deposits occur close to the entrance. The cemented deposits form a mound-like feature at the cave entrance, presently west of the drip line (i.e., outside the cave; Fig. 1c; Extended Data Fig. 1). The layers of the cemented deposits are sub-horizontal and are truncated on the west forming a slope, indicating erosion or mass-movement. Erosion of the cemented deposits is likely a still on-going process. The deposits are cemented by secondary calcite mainly composed of fire residues, stones, bones, and anthropogenic artifacts.

The cave entrance is 8 m wide and 3.5-4 m high. The vertical walls of the cave extend a few meters westward beyond the entrance dripline, and together with collapsed limestone fragments found within the cemented sediments, the indicate the past continuation of the cave, where the ceiling had collapsed. This part of the site is termed here as the cave Terrace. The chimney and the current opening of the cave seem to have allowed some terra rossa colluvium to enter the cave, due to their mid-slope setting. Thus, terra rossa soil that occurs on the hill above the cave entered into it (nowadays and in the past) either from the chimney or next to the dripline and westwards of it.

S2. Tinshemet Cave stratigraphy

The Terrace (Fig. 1, Extended Data Fig. 1)

Unit A (ca. 0.8 m thick): is composed of light grey cemented sediments containing mainly calcite with some clay, quartz and carbonated hydroxylapatite. It was further subdivided into five archaeological layers (~15-25 cm each) according to density of the archaeological remains and presence or absence of natural stones that represent cave roof and wall fragments (A1-A5). A2 and A4 are rich anthropogenic units containing lithic artifacts, faunal remains, ochre fragments and human remains (Layer A2). Layers A1, A3 and A5 exhibit low density of anthropogenic remains. The particle size distribution (PSD) of the detrital grains (carbonate free) of unit A is bimodal, with relatively equal amplitude of the two modes: 1) coarse sand mode at 500-1200 µm, composed mostly of angular fragments of flint and ochre, with few sub-angular quartz grains, and 2) coarse silt mode at 44-60 µm, composed of angular to sub-angular grains, mostly quartz, cemented by clay minerals. A subtle mode appears also in the submicron fraction, related to clay minerals.

Unit B (ca. 0.4 m thick) is characterized by light brown-grey cemented sediments. The sediments are slightly more brownish due to higher amount of clay than in the overlying Unit A. Human remains, together with lithic artifacts, faunal remains and ochre chunks have been especially abundant in this Unit. Unit B was sub-divided into sub-layers B1a and B1b. B1a is the richest layer of the site containing dense lithic and faunal assemblages, ochre and articulated remains of human adult individual (Figs. 1-2). The PSDs of unit B is similar to those of unit A, with a lightly finer silt mode, centered at 41-43 µm.

Unit C (ca. 0.5-0.7 m thick) is characterized by light brown-grey cemented sediments and has a significantly low density of remains and large amounts of stones. Phosphatization of the limestone bedrock indicates past presence of bat guano, suggesting that the roof of the cave extended further west during accumulation of Unit C. The deposit just above this phosphatized bedrock was found to be rich in fossil pollen grains. The PSD of unit C differ from those of the upper units as it is unimodal, showing mainly the coarse silt mode, with a small, subtle fine-medium sand mode at ~200-300 µm. No coarse sand mode (related to human activity) was identified.

The First Chamber (Fig. 1, Extended Data Fig. 1)

Layer I (0.2-0.3 m. thick): Topsoil layer which is a mixed brown soft sediment containing lithic artifacts, and modern micro-fauna (i.e., bats). The lithic artifacts deriving from the topsoil layer characterize only a MP period. Between 20 and 25 cm of topsoil were removed before reaching the first intact archaeological layer. The topsoil, and to a lesser extent layer II, have been disturbed by roots of a fig tree that grows at the entrance of the cave.

Layer II (0.2-0.3 m thick): Light brown soft sediment mostly composed of clay with a lesser amount of calcite, quartz and carbonated hydroxylapatite. It is basically the same sedimentological and archaeological composition as Layer III, however, it contains some roots that might have disturbed the deposits.

Layer III (ca. 0.7-1 m. thick): Light brown soft sediment mostly composed of clay with a lesser amount of calcite, quartz and carbonated hydroxylapatite. This layer might appear slightly more cemented below the dripline. Layer III is the main MP archaeological deposit in the First Chamber, containing flint artifacts, faunal and human remains, including an articulated skeleton of a child and the remains of an adult (part of the calvaria).

DB layer. Inside the First Chamber a soft non-anthropogenic accumulation (0.2-1 m thick), composed of compact dark brown (henceforth DB layer) sediments (Fig. 1). This layer contains few lithic artifacts (often rolled and patinated) and a small amount of faunal remains sometimes mixed with modern and fossil micro-fauna.

S3. Geoarchaeology

Two types of sediments were observed during excavations at Tinshemet Cave: loose reddish brown and cemented grey-coloured sediments (Supplementary Table 1). A clear spatial partition is visible in their distribution across the site, with the loose reddish-brown sediments concentrated inside of the cave and the cemented grey sediments appearing in the outer part of the First Chamber and extending further outside forming a terrace. The grey sediments close to the cave's opening are slightly more friable than those found on the external Terrace. In addition to variations in the types of sediments, significant differences are also apparent in the concentrations of anthropogenic remains within these two areas; while in the outer part of the First Chamber finds are scarcer, the remains of anthropogenic activities are prevalent across the Terrace (Extended Data Fig. 2).

Mineralogical compositions of the sediment samples from the inner part of the First Chamber (layer DB; n=57) are dominated by unheated (geogenic) clay and occasionally contain lesser amounts of calcite, quartz, and carbonated hydroxylapatite. The latter minerals are nearly or completely absent from sediment samples collected from areas further inside of the cave, which were found to be devoid of evidence for anthropogenic activities, while these minerals are more prominent in samples taken from near the cave's entrance (Layer III) where anthropogenic remains were identified. The clay and quartz components in these loose reddish-brown deposits are understood to originate from terra rossa soil that infiltrated into the cave from its chimney by gravitational dry and wet flows. The calcite component in these deposits may be attributed to fragments of cave wall and ceiling (the limestone Bina Formation). The carbonated hydroxylapatite component may originate from bone fragments and/or authigenic phosphate nodules from degradation of bat guano (a colony of fruit bats currently resides in the internal part of the cave).

Mineralogical compositions of sediment samples collected from the Terrace outside of the cave (n=218) are dominated by calcite with lesser amounts of unheated (geogenic) clay, quartz, and carbonated hydroxylapatite. Calcite here may originate from wood ash, cave wall/ceiling fragments, tuffa, and secondary reprecipitated calcite responsible for the induration of the Terrace deposits. The clay and quartz components originate from wind-blown dust and from terra rossa that mixed with this calcitic deposit (infrared spectra often show higher absorption bands of clay in reddish-grey sediment samples, indicating higher amounts of clay minerals). The carbonated hydroxylapatite originates from the abundant bone fragments in the deposits.

Quantification of ash pseudomorphs and phytoliths from the sediment samples (n=68) showed these micro-remains to be nearly absent across the site. In sediment samples from both inside and outside of the cave average phytolith and ash pseudomorph concentrations fell well below 1 million per 1 gram of sediment. The highest concentration of ash pseudomorphs found is 1.17 million per 1 gram of sediment identified on the Terrace while the maximum concentration of 0.26 million ash pseudomorphs per 1 gram of sediment is obtained from a sample from inside of the cave. Phytoliths and ash pseudomorphs appeared pitted and cracked.

Burn colour codes of bone fragments from across the site show the presence of all colour codes, implying the presence of unburned/slightly burned (yellowish, cream), lightly burned (light brown), fully carbonized (black), and partially (grey) to fully calcined (white) bones. The majority of the bone fragments inside of the cave (50%) and from the Terrace (60%) are unburned to lightly burned (burn colour codes 1-2). Bone fragments exhibiting clear-cut carbonization (burn colour codes 3-4) make up 36% and 26% of the fragments studied from inside of the cave and the Terrace, respectively. Bone fragments with clear-cut calcination (burn colour codes 5-6) form 14% of the fragments studied in both areas of the site (Extended Data Fig. 2).

Based on these data, the deposits at the site exhibit two different paths of formation processes. Reworked terra rossa dominates the DB layer with no evidence for ash or heated clay. These reddish-brown loose deposits have low frequencies of anthropogenic remains and no indications for authigenic minerals typical of highly acidic conditions (e.g., taranakite;[6]). This implies that the low artifact concentration is original, reflecting little use of the internal part of the cave by hominins. On the other hand, the artifact-rich cemented grey deposits of the Terrace and the outer part of the First Chamber suggest that the sediments composing this area of the site likely consisted of ash and an accumulation of other fire residues. This hypothesis is further supported by the presence of microcharcoal, carbonized and calcined bone fragments, and ash pseudomorphs. These remains of combustion activities were likely affected by water in the active karstic cave system. The presence of well-preserved bone features together with the absence of authigenic phosphate minerals indicative of high acidity suggest that dissolution of ash and reprecipitation of secondary calcite occurred under neutral to alkaline conditions. This process eliminated most wood ash pseudomorphs, expressed by relatively low concentrations of ash pseudomorphs (0.22 million per 1 gram of sediment on average; to be compared with tens of millions per 1 gram of fresh wood ash;[7]). Moreover, the alkaline hydrological conditions probably caused almost complete dissolution of phytoliths[8]. In short, the low concentrations of ash pseudomorphs and phytoliths are likely a result of extensive partial dissolution of these micro-remains, thus removing them from the archaeological record, rather than a result of their absence at the site in the first place. This scenario is consistent across the site, based on the analysis of 68 sediment samples. A similar situation was previously identified at Qesem Cave located slightly to the north of Tinshemet Cave in the same region[9]. The presence of unheated clay in the Terrace deposits despite evidence for extensive combustion activities may be explained to be the result of mixing of unheated terra rosa clay with the heated deposits[10].

Supplementary Table 1. Micromorphological observations. Summary of mineralogical, phytolith, ash pseudomorph, and micro-bone analyses.

Excavated Unit	Number of Bulk Sediment Samples (2017-2021)	Sediment Description	Bulk Mineralogy	Number of samples subjected to micro-remain quantification	Percentage of Samples Subjected to Micro-Remain Quantification (%)	Phytoliths Average Concentration (million per gram sediment) with Std.	Ash Pseudomorphs Average Concentration (million per gr. sediment) with Std.	Number of Micro-Bones Analyzed	Percentage of Micro-Bones Burn Color Code 1-2 (%)	Percentage of Micro-Bones Burn Color Code 3-4 (%)	Percentage of Micro-Bones Burn Color Code 5-6 (%)
First Chamber (DB Layer)	57	Loose, red-coloured, fine-grained clayey sediment	Clay (unheated), calcite, quartz, carbonated hydroxylapatite	9	13.24	0.02 +/- 0.04	0.00 +/- 0.00	14	50	36	14
First Chamber (Layer III)	46	Loose, red-coloured, fine-grained clayey sediment intercalating with friable, grey-coloured sediment	Clay (unheated), calcite, quartz, carbonated hydroxylapatite	18	26.47	0.01 +/- 0.02	0.05 +/- 0.07	3	67	33	0
Terrace (Units A and B)	204	Cemented, grey-coloured sediment	Calcite, clay (unheated), quartz, carbonated hydroxylapatite	41	60.29	0.00 +/- 0.02	0.27 +/- 0.32	127	60	26	15

S4. Palynology

All archaeological samples collected from the cemented deposits were pollen barren (samples nos. 1–8; Supplementary Table 2). A yellowish-greyish sample taken from the crust above bedrock in the lowermost unit (Unit C, samples nos. 9-10) was characterized by a good state of pollen preservation and relatively high taxa diversity. The palynological spectrum of this rich sample is comprised of Mediterranean trees (in declining order): olive (22.5%), Aleppo pine (16.7%), buckthorns (16.3%), evergreen oak type (4.4%) and deciduous oak type (3.5%). The group of non-arboreal vegetation, composed of small shrubs and herbs, is dominated by members of the goosefoot family (8.4%), parsley family (6.6%) and aster-like pollen type (4.0%). The assemblage includes several fruit trees such as carob, grape, date palm, buckthorns and fig.

The control samples were not very useful. The recent guano sample mainly included pollen from a non-local origin such as *Pseudobomba* (bombax), *Mangifera* (mango), *Psidium* (guava), *Eugenia* (pitanga) and *Acca* (Feijoa). Today the cave is occupied by fruit bats that apparently consume mainly exotic fruits of tropical origin. The recent surface sediment sample contained many spores and only a few pollen grains (chenopods, pine, *Eucalyptus*). The presence of these tree taxa is most likely due to modern afforestation rather than representing the natural flora. The site is located at the foothills of the Shephelah (plain), an area that has been subject to thousands of years of human disturbances. Similar to other Mediterranean areas in the southern Levant, the intensity of human interference increased dramatically in the last 100 years due to modern agriculture, forestry and development. Human interference completely transformed the vegetation of the region into an artificial environment. Hence, the contribution of the recent pollen samples to the interpretation of the fossil pollen data is very limited.

Supplementary Table 2: Palynological samples from Tinshemet Cave.

	Lab ID	Stratum	Field ID	Context/description	Results
1	P.#1/2021	A2	Sq. I22/a B.863	Breccia, near Homo 8	No pollen
2	P.#2/2021	A3	Sq. I24/b B.925	Breccia	No pollen
3	P.#3/2021	A4	Sq. A25/b B.875	Breccia	No pollen
4	P.#4/2021	B1a	Sq. AH24/c B.814	Breccia	No pollen
5	P.#5/2021	B1b	Sq. AF 23/c B.922	Breccia	No pollen
6	P.#6/2022	A2	Sq. AI22/b B.986	Breccia, near T8	No pollen
7	P.#7/2022	A4	Sq. AG22/d B.970	Breccia	No pollen

8	P.#8/2022	B1a	Sq. AH24/b B.1002	Breccia	No pollen
9	P.#9a/2022	C	Sq. AF25/d	Crust above the bedrock at the bottom of Unit C (guano?)	High pollen concentrations
10	P.#10/2022		Control	Recent Guano (inside the cave)	Very high pollen concentration, mainly from exotic origin
11	P.#11/2022		Control	Surface sediment (near the cave)	Very low pollen concentrations, many spores

Samples collected from Tinshemet Cave during seasons 2021 and 2022 for palynological investigation.

The pollen-bearing deposit: The good state of pollen preservation and the relatively high taxa diversity of the sample associated with the cave's bedrock (no. 9, Supplementary Table 2) demonstrates that this context can be very useful in palaeoecological research. The sample is associated with phosphatized bedrock indicating processes related to degradation of bat guano[6], and thus it may cautiously be suggested that the pollen in this sample may be related to guano of bats that dwelled in the cave (during the period of accumulation of Unit C). If correct, it indicates that the guano was fossilized under favourable environmental conditions that allowed the preservation of pollen, as was already shown in previous studies[11–13]. Often, organic matter, including pollen, is relatively well preserved in fecal deposits due to mineralization processes under slightly acidic conditions, as also suggested by the phosphatic mineralization of the cave bedrock[6,14–16]. Pollen exines are generally resistant to degradation by digestive enzymes[17], and the pH of the digestive system is relatively low (4–6)[12]. Several studies have described the mechanisms for the incorporation of pollen into bat guano: (i). Pollen in fragments of bat skin and hair lost during grooming[18]; (ii). Dust brought onto guano by air currents[19]; (iii). Through drinking water and inhaling; and (iv). Direct ingestion of insects that are themselves covered by pollen, or whose digestive system contains pollen[18,20]. The latter factor may explain the relatively high ratios of the insect-pollinated tree buckthorns (16.3%).

Although bats can migrate hundreds of kilometres, they rarely forage further than a few kilometres from their shelter[12]. One can therefore expect that the palynological spectrum presented in this study is mainly representative of plants growing in the vicinity of Tinshemet Cave. Pollen grains of several fruit trees were detected in the pollen assemblage: grape, date palm, fig, carob and buckthorns. This important observation sheds light on the fruit-gathering opportunities which were available for the hunter-gatherer community which occupied Tinshemet Cave.

S5. Thermoluminescence (TL) dating

Supplementary Fig. 1: Internal (alpha + beta) dose-rate as a function of the paleodose.

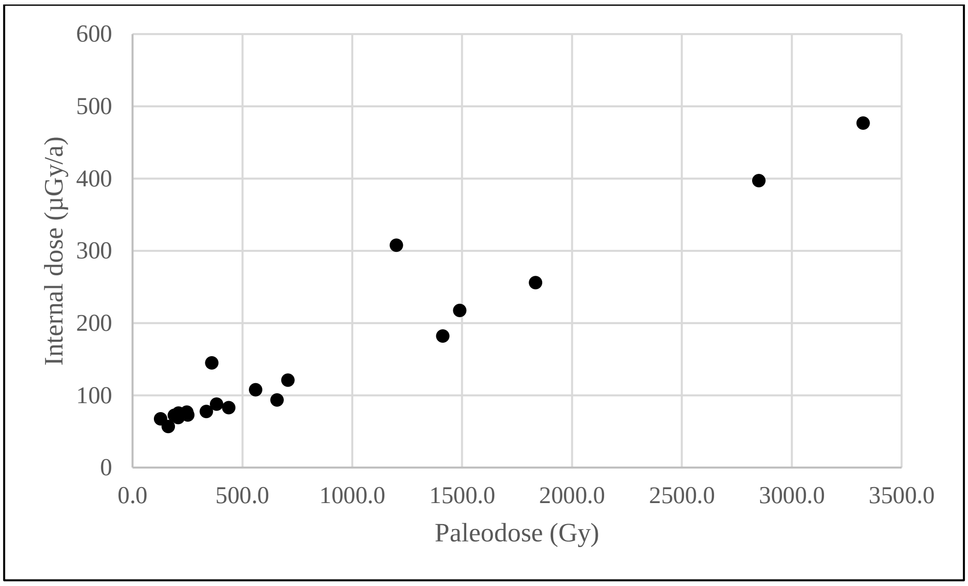

Each data point is a single measurement. The errors on the Paleodoses range from 5% to 12% and on the Internal Doses from 2.1% to 4.6 % (see Extended data Table 1).

S6. Optically Stimulated Luminescence (OSL) dating

Supplementary Fig. 2: Luminescence dating results.

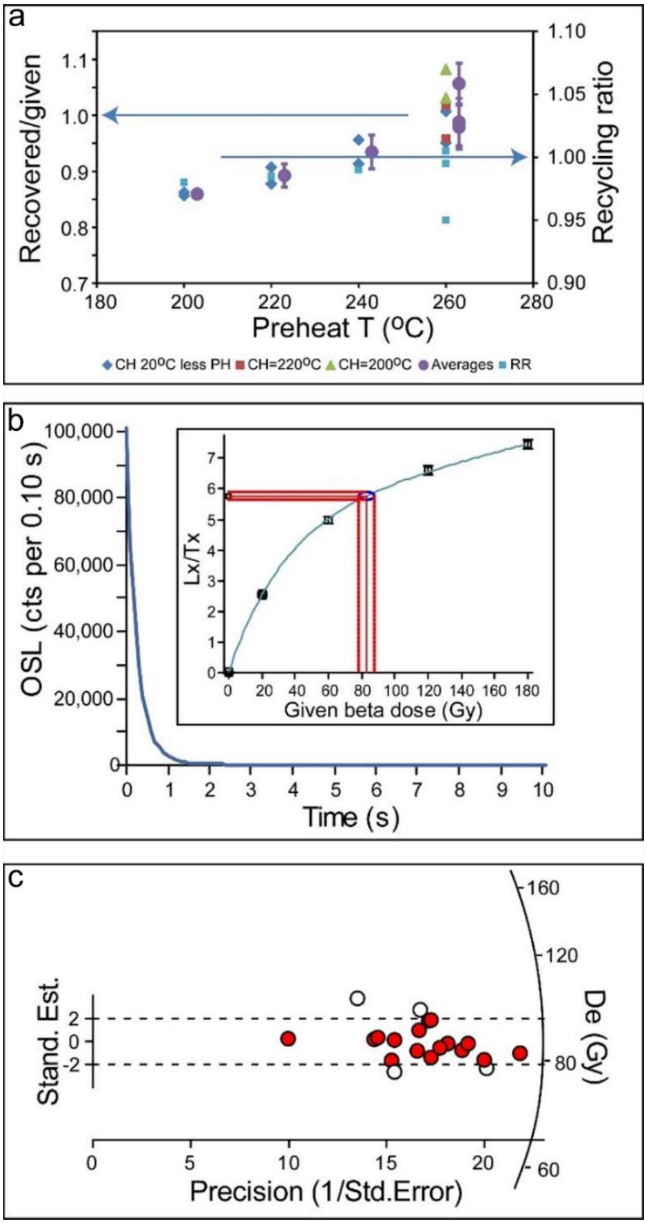

a. Dose recovery over a range of preheat (PH) and cutheat (CH) temperatures. PH ranged from 200°C to 260°C and CH from 180°C to 240°C, with different combinations. Two measurements were performed for each combination. Data are also presented as mean values (violet dots) ± standard deviation. Recovery ratios are shown on the left y-axis. Recycling ratios (RR- right y-axis) are solid blue squares, with the x-axis shifted for clarity. The best recoveries of 0.98 were obtained using a PH-CH combinations of 260°C-220°C and 260°C-240°C (red squares and blue diamonds, respectively). **b**, Natural OSL signal for one aliquot of sample TNS-15, showing 10 s out of a 40 s measurement. Note rapid decay to background within <2 s. Inset: the dose response curve (DRC) for the same aliquot, an exponential+linear fit gives a De of 86±5 Gy. The dose point at 20 Gy consists of two repeated (recycling) points. **c,** A radial plot of all aliquots measured for sample TNS-15 (N=20). Note tight and normal distribution. Overdispersion of the measurements is 8%, and the De for the sample is 86±2 Gy, calculated using the central age model.

S7. Uranium (U)-series dating

Secondary calcite. Detrital thorium concentration was found to vary between 100 ppb to less than 5 ppb, except in small circular areas likely filled with clays having a high ^{232}Th content, which were therefore defined as ROEs (Region Of Exclusion) and discarded from further analysis. A segmentation of the image according to the variations of the (^{232}Th/^{238}U) ratio was carried out, thus making possible the virtual creation of sub-samples. In each sub-sample, the isotope ratios (^{230}Th/^{232}Th), (^{234}U/^{232}Th) and (^{238}U/^{232}Th) were calculated and diagrams of (^{230}Th/^{232}Th) versus (^{234}U/^{232}Th) and (^{234}U/^{232}Th) versus (^{238}U/^{232}Th) were created. These isochron plots allowed to determine the detrital thorium fraction incorporated during the formation of the speleothem. In addition, the curves (^{234}U/^{232}Th) versus (^{238}U/^{232}Th) obtained for the two speleothems lead to similar initial (^{234}U/^{238}U) ratios: 1.071±0.002 for Tin19FS2 and 1.062±0.003 for Tin19FS3, as expected.

Snail shells (Extended Table 3). The (^{234}U/^{238}U) ratio is rather constant (about 1.2) with the exception of one area of the Tin19SSh7 sample where this ratio drops to 1.07. This difference could be explained by local leaching of uranium in this sample, which was therefore excluded from further analysis. In contrast, sample Tin19SSh9 shows high levels of ^{238}U concentrated around numerous cracks, which could be explained by local uranium enrichment around these areas. This sample was therefore also excluded. The ^{232}Th contents in the other samples are very low and homogeneous within the shell, with the exception of some detrital thorium incorporations in the cracks and on the edges of the samples. These areas were identified during image processing and indicated as ROEs. In the rest of the shells, the detrital fraction is negligible, with (^{230}Th/^{232}Th) activity ratios > 500.

S8. Cryptotephra

Tinshemet Column 1 (Terrace; Supplementary Fig. 3)

Within the Tinshemet Column 1 sequence, very low shard abundance was identified in a single tephra concentration zone spanning a 20cm interval (87.84-87.64m datum) within the very hard breccia, ranging between 0.43 s/g to 1.52 s/g. Glass shards were colourless with some cuspate features. Further analyses pinpointed the highest concentration within the 5cm interval from 87.79-87.74m datum, designated as **TIN-C1-TZ1**. Despite these extremely low counts, compositional data was successfully obtained from a single glass shard which yielded an evolved rhyolitic signature.

Supplementary Fig. 3: Locations of sediments sampled for tephra analysis in the Terrace of Tinshemet Cave.

West-East view of the terrace with excavated squares. The locations of tephra columns 1-4 are indicated.

Tinshemet Column 5B (First chamber; Supplementary Fig. 4)

Inside the cave, very low shard abundance (0.48 s/g) was found in a single tephra concentration zone spanning a 10cm interval (between 87.16-87.26m datum) within Layer III. Glass shards were mostly colourless although at least one shard was observed with a slightly darker pink hue. Further analyses pinpointed the highest concentration within the 5cm interval from 87.16-87.21m datum, designated as **TIN-C5B-TZ1**. Despite these extremely low counts, glass chemical data was obtained from two shards, one showing an evolved rhyolitic signature **TIN-C5B-TZ1a**, and the other exhibiting slightly lower SiO_2 wt. % totals but can still be classified as a rhyolite **TIN-C5B-TZ1b**.

Supplementary Fig. 4: Locations of sediments sampled for tephra analysis in the First Chamber of Tinshemet Cave.

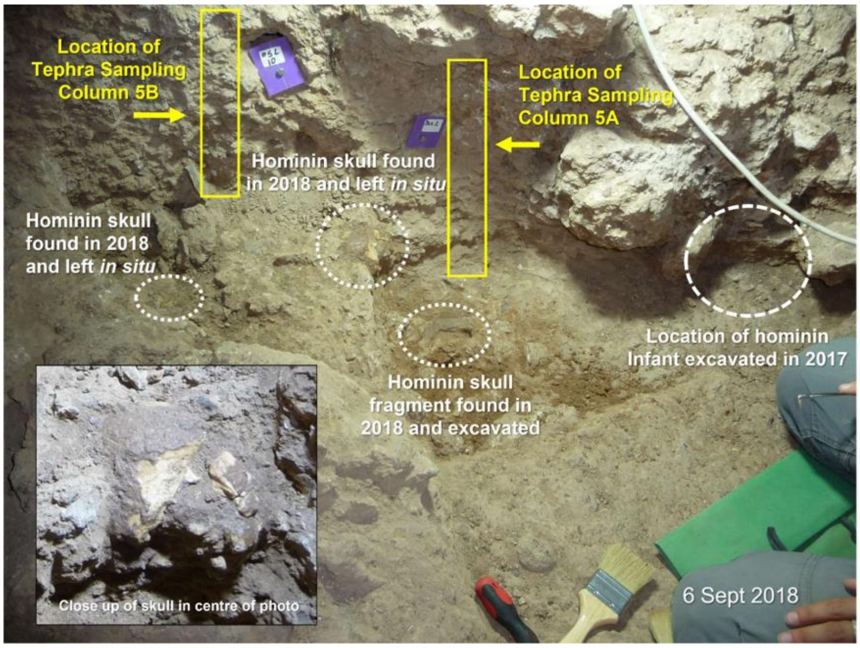

Section within the first chamber showing sampling locations of sediments for tephra analysis (tephra columns 5A and 5B) near the burial of *Homo*1 (details appear in the small black square on the left corner of the figure).

The two, more evolved glass shards (TIN-C1-TZ1a & TIN-C5B-TZ1a) bear some similarity to one another, enough so perhaps, to propose that these form a correlation across Column 1 and Column 5 from which they are found. They also exhibit a glass chemical signature that is similar to volcanoes from the Aegean Arc, such as Kos, but also centres situated in Central Anatolia (e.g., Acıgöl). Despite the differing geological settings of these volcanoes, the evolved products are very similar, particularly when only major and minor elemental analyses are considered. Several authors have noted the difficulty in chemically distinguishing these systems, however, for the approximate time period in question (ca. 100-130 ka) and based on current understanding of the Aegean and Central Anatolian volcanoes eruptive history, identifying glass shards of this chemical composition is relatively unusual and perhaps significant.

Recent work by Barzilai et al.[21] has established a tephrostratigraphic link between Nahal Aqev and two marine core sites in the eastern Mediterranean using a single tephra that exhibits a similarly evolved rhyolitic signature to the two aforementioned shards recovered from Column 1 and Column 5. It is possible that TIN-C1-TZ1a & TIN-C5B-TZ1a are also part of this tephra layer which has been dated to 126.4 ± 2[22,23]. The two shards match consistently with the Nahal Aqev tephra in some major element plots, e.g., SiO_2, TiO_2, Al_2O_3 wt. % (Supplementary Fig. 5), however, plots of other elements, e.g., CaO and total iron (FeOt) wt. % andthe alkalis are less convincing (Supplementary Fig. 6).

Supplementary Fig. 5: Major elements of SiO_2, TiO_2, Al_2O_3 wt. % in the tephra from Tinshemet Cave compared with Nahal Aqev, the Aegean Sea core (LC21-993.5) and from the Levantine Sea core (ODP967-129.5).

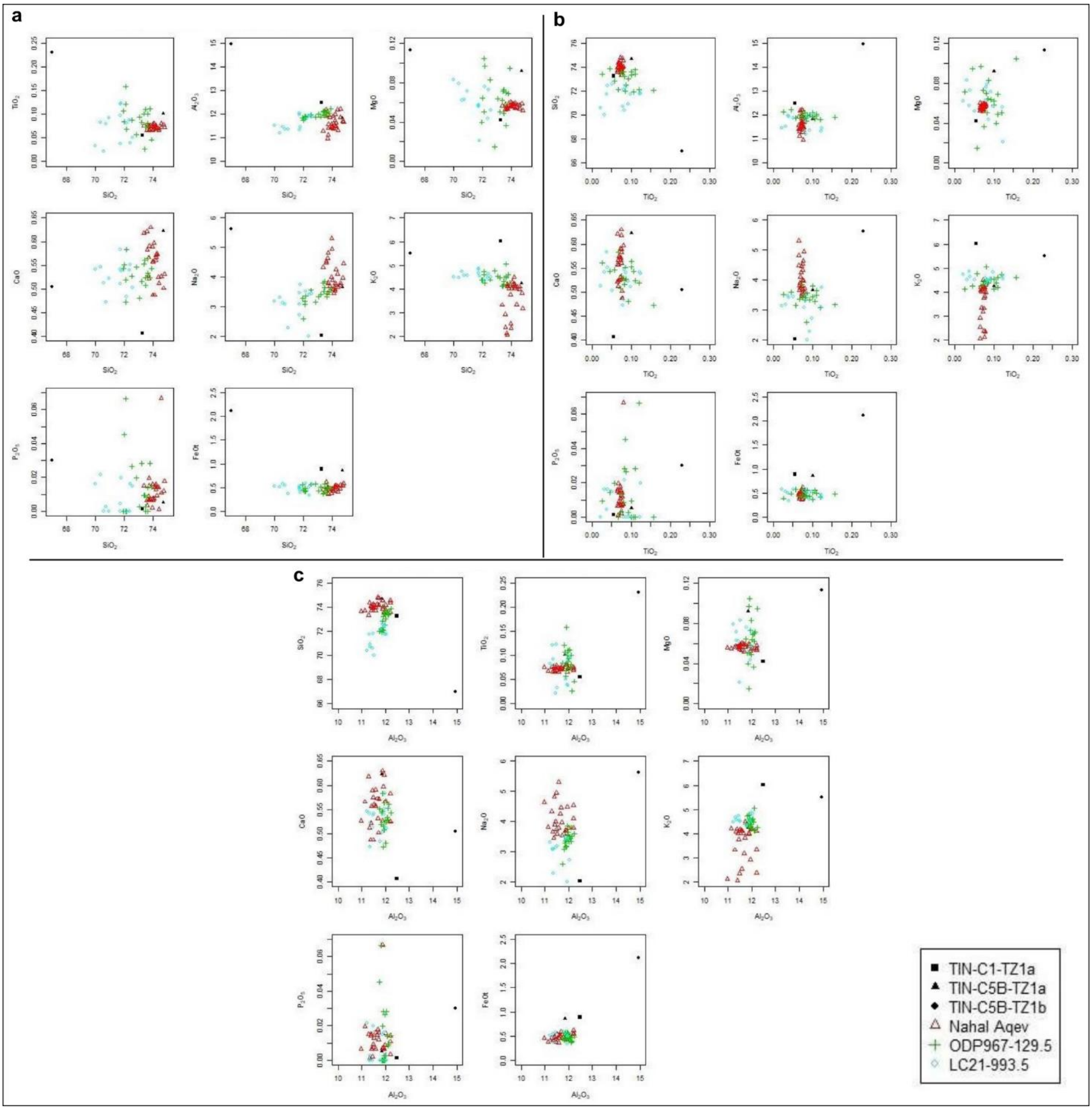

a, Multiple plots of SiO_2 *vs*. TiO_2, Al_2O_3, MgO, CaO, Na_2O, K_2O, P_2O_5, FeOt. **b**, Multiple plots of TiO_2 vs. SiO_2, Al_2O_3, MgO, CaO, Na_2O, K_2O, P_2O_5, FeOt. **c,** Multiple plots of Al_2O_3 *vs*. SiO_2, TiO_2, MgO, CaO, Na_2O, K_2O, P_2O_5, FeOt.

Supplementary Fig. 6: Major elements of CaO, FeO wt. % and the alkalis in the tephra from Tinshemet Cave compared with Nahal Aqev, from the Aegean Sea core (LC21-993.5) and from the Levantine Sea core (ODP967-129.5).

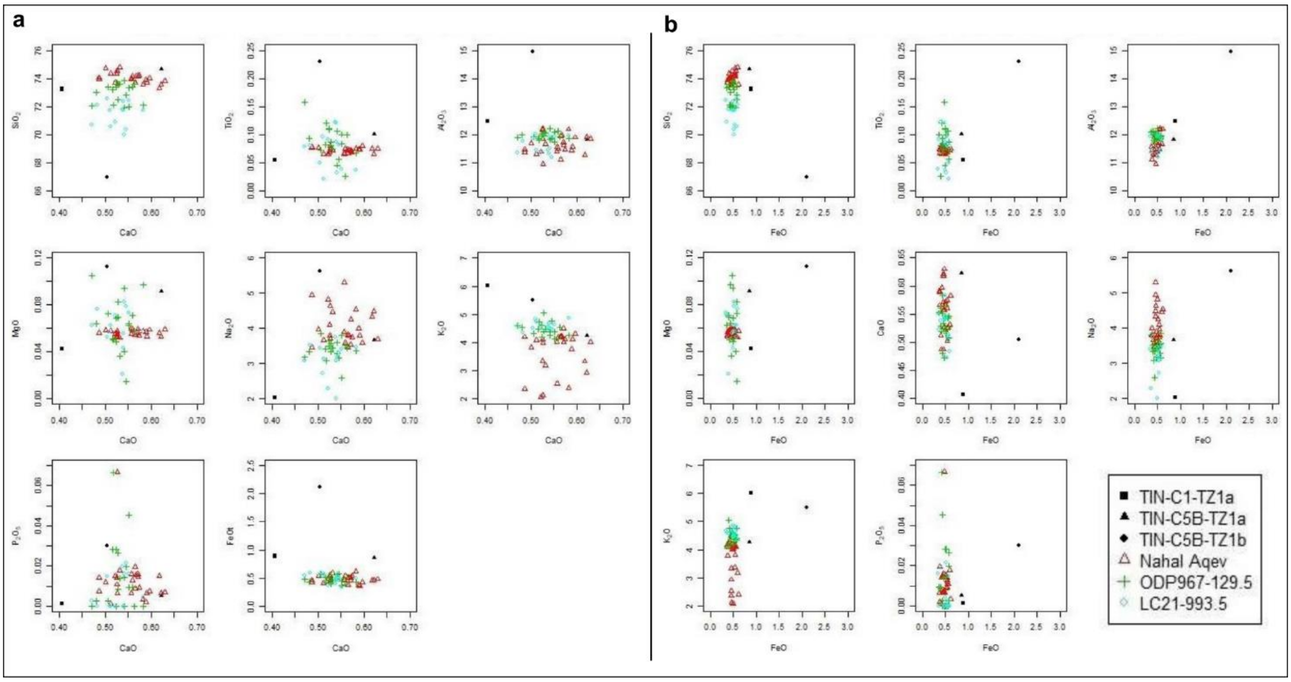

a, Multiple plots of CaO vs. SiO_2, TiO_2, Al_2O_3, MgO, Na_2O, K_2O, P_2O_5, FeOt. **b**, Multiple plots of FeOt vs. SiO_2, TiO_2, Al_2O_3, MgO, CaO, Na_2O, K_2O, P_2O_5.

S9. Micromammals remains

The combined MNI-based relative abundance of *Mastomys* and *Arvicanthis* at Tinshemet (12.8%) falls within the range of variability of the ten Qafzeh layers (2.3–14%, avg. = 5.8 ± 1.8%; taxonomic abundance data from Rabinovitch and Tchernov[24]: Table 1), considering only the Rodentia (Supplementary Fig. 7; Supplementary Table 3). The proportion of these taxa in the Tinshemet assemblage most closely resembles that of Qafzeh Layers XX and XXI (14 and 10.8%, respectively; or a 1:7 and 1:9 retrieval ratio), while it is considerably lower in other Qafzeh layers (2.3–6.6%, avg. = 4.19 ± 0.8). It is noteworthy in this respect to note the much lower proportions of *Mastomys* and *Arvicanthis* in early-MP microfaunal assemblages of Hayonim Layer E (0.2%;[25]: Table 2) and Misliya (1.2%;[26]: Table 2), and the absence of these two taxa in microfaunal assemblages of other MP phases (Tabun Layer C and Rantis cave from the late early MP and Kebara Layers VI–XII and Amud Layers B4–B2 from the late MP;[27]: Table 1;[4]: Table 4;[25]: Table 2;[28]). The taxon *Mastomys*, furthermore, is among the highest in rank abundance within the Qafzeh layers (2nd–4th most abundant taxon), as is the case with the Tinshemet assemblage (3rd most abundant taxon), while it is fairly rare in early-MP assemblages (ranked 9th and 10th at Hayonim Layer E and Misliya, respectively).

Differences in taxonomic composition between the Tinshemet and Qafzeh assemblages may be attributed to sampling issues or within-region environmental and ecological variability between the relatively precipitation-rich Upper Galilee location of Qafzeh and the drier Shephelah location of Tinshemet. Interregional variability may account for the absence of the woodland taxon *Myomimus* at Tinshemet, while it is fairly well represented at Qafzeh (3.3% in total). The absence of the open woodland taxon *Sciurus* and the rocky-habitat *Gerbillus* at Tinshemet may be a sampling artifact, as these taxa are very rare at Qafzeh (0.1 and <0.1%, respectively). Cricetid taxa (*Mesocricetus auratus* and *Cricetulus migratorius*) are absent at both cave sites, an observation which was emphasized in the case of Qafzeh given the consistent presence of these two taxa through other phases of the mid–late Pleistocene, and the fact that they are part of the extant mammalian community of the region in the present interglacial[25].

Supplementary Table 3: Micromammals taxonomy at Tinshemet Cave.

Micromammals	NISP			MNI		
	No.	Relative abundance %	Rank abundance	No.	Relative abundance %	Rank abundance
Rodentia						
Apodemus sp.	2	0.87	6	1	1.15	5
Arvicanthis sp.	3	1.31	5	3	3.45	4
Mastomys sp.	9	3.93	3	5	5.75	3
Meriones sp.	17	7.42	2	14	16.09	2
Microtus sp.	179	78.17	1	53	60.92	1
Mus sp.	1	0.44	7	1	1.15	5
Spalax sp.	6	2.62	4	3	3.45	4
Eulipotyphla						
Crocidura sp.	12	5.24		7	8.05	
Total	229			87		

Relative abundance (%) and rank abundances of micromammals at Tinshemet Cave, based on numbers of identified specimens (NISPs) and minimum numbers of individuals (MNIs).

Supplementary Fig. 7: Fossil molar teeth of African-tropical index fossil taxa *Mastomys* (a–f) and *Arvicanthis* (g–i) from Tinshemet Cave.

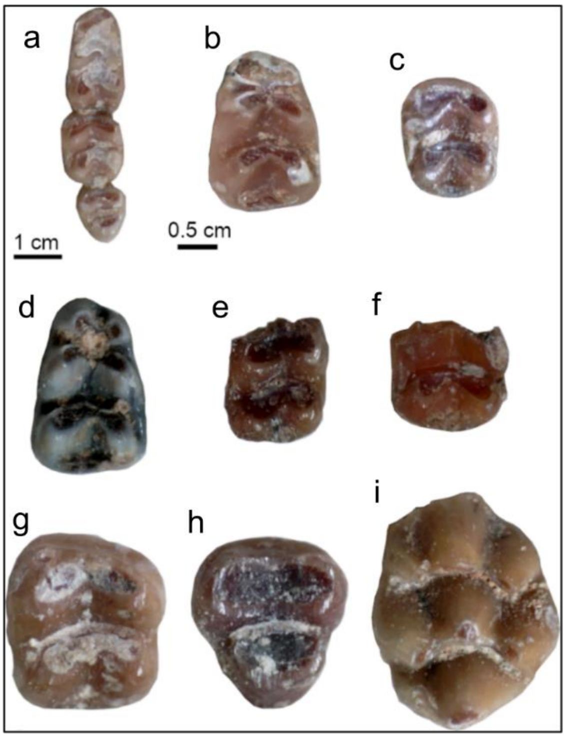

a, complete left tooth row (m1–3); **b**, right m1; **c**, left m1; **d**, right m1, burned; **e**, left posterior m1, broken; **f**, left posterior m1, broken; **g**, left m2; (H) left m3; **i**, right M1. Note the different scales for **a** (1 cm) and **b**–**i** (0.5 cm).

Molar length measurements were taken from all sufficiently preserved specimens and compared to ranges obtained for fossil material from early-MP Misliya[26] and late Lower Palaeolithic Qesem[29] and Oumm Qatafa caves[30], from which relevant regional data is presently available (Supplementary Table 4). These data show that two m1s of *Mastomys* are closely comparable in size to two such specimens from early MP Misliya, while two m2s are somewhat smaller than one such tooth from Misliya ([26]: Table S3). Molars of *Arvicanthis*, an M1 and m1, are slightly smaller than such teeth from Oumm Qatafa, and an m2 and M3 are somewhat larger than such teeth ([30]: Table 6). One *Apodemus* m1 tooth should be assigned to the small-sized wood mouse *A. flavicolis* (see[26]: Table S3;[29]: Table 2). Three shrew molars, one m1 and two m2s, fall within the range of fossil specimens from Misliya and indicate an assignment to *Crocidura* sp., while another m1 is slightly above that range, an m2 is well below that range, and several other specimens could not be assessed due to lack of comparative measurement ranges. Molars of other taxa are broadly comparable in size with the fossil material considered here.

Taphonomic indications were collected for both human (burning) and non-human (digestive) impacts (Supplementary Fig. 8). Predator digestion marks of predominantly light grades (mostly slight rounding of the occlusal edges of the tooth salient angles) were observed on 30 *Microtus* molars of a total of 216 such teeth in the assemblage (13.9%), indicating the effect of a low-impact collection agent, most likely the ubiquitous barn owl *Tyto alba*. Also, 11 skeletal remains showing complete blackening or calcination due to exposure to what were likely human made fires were detected, revealing a relatively low rate of exposure within the entire studied assemblage of cranial specimens (4.8%). The observed modifications suggest an accumulation of the remains of small mammals at Tinshemet by a nocturnal bird of prey, as has been amply documented at other regional prehistoric cave sites, with subsequent incidental exposure to fire, possibly within human-maintained hearths (for comparison, see e.g.,[31] [41.3% digested; 8% burned];[26] [23% digested; 13% burned]).

Biostratigraphic considerations place Tinshemet at the time of the Qafzeh mid-MP deposits, in agreement with the absolute age determinations and lithic analysis presented here. The recently revised biostratigraphic framework of the south Levantine MP builds upon the alternating sequence in which two key index fossil taxa occupied the region. Thus, four discrete biozones covering the MP timespan are delineated according to the presence or absence of the African-tropical rodent taxa *Mastomys* and *Arvicanthis* (Biozones V–II), each represented by the major units of deeply-stratified cave sequences[26]: Biozone V, occurrence of *Mastomys* and *Arvicanthis* at the beginning of the early MP period (c. 250–170 ka; Misliya, Hayonim Layer E and Tabun Layer D); Biozone IV, absence of the two taxa in the late part of the early MP (170–130 ka; Tabun Layer C and Rantis); Biozone III, recurrence of these taxa in the mid-MP (130/120–80 ka; Qafzeh Layers XV–XXV and Tinshemet); and Biozone II, final regional extirpation of *Mastomys* and *Arvicanthis* within the late MP (80–50 ka; Kebara Units VI–VII and Amud Layers B4–B2). Further consideration of quantitative data on species relative and rank abundances indicates the possibility that at least the part of the Tinshemet deposits exposed so far may correlate with Qafzeh Layers XX or XXI, wherein *Mastomys* and *Arvicanthis* are comparatively superabundant.

Supplementary Table 4. Molar tooth length size (mm) of various species of rodents in Levantine Lower and Middle Paleolithic sites.

			Measurements (mm)				
Taxon	**Element**	**Part**	**This study**	**Fossil material**	**Source**	**Site**	**NISP**
Spalax	Molar	M1	2.552	2.35–2.60	[30]: Table 4c	Oumm Qatafa	12
Spalax	Molar	M1	2.249	2.35–2.60	[30]: Table 4c	Oumm Qatafa	12
Spalax	Molar	M1	1.547	2.35–2.60	[30]: Table 4c	Oumm Qatafa	12
Spalax	Molar	M2	1.994	1.95–2.30	[30]: Table 4c	Oumm Qatafa	11
Spalax	Molar	m3	1.826	1.78–2.24	[29]: Table 2	Qesem	2
Mus	Molar	m1	1.183	0.90–1.69	[29]: Table 2	Qesem	15
Meriones	Maxilla	Complete tooth row	4.635				
Meriones	Molar	m1	2.568	2.29–2.84	[29]: Table 2	Qesem	11
Meriones	Molar	M1	2.355	2.54–3.23	[29]: Table 2	Qesem	15
Meriones	Molar	M1	2.337	2.54–3.23	[29]:Table 2	Qesem	15
Meriones	Molar	M2	1.207	1.45–1.71	[29]: Table 2	Qesem	8
Meriones	Molar	M3	0.69	0.84	[29]: Table 2	Qesem	1
Mastomys	Mandible	Complete tooth row	4.585				
Mastomys	Molar	m1	2.249	1.75–2.054	Small specimen: [30]: Table 7c; large specimen: [26]: Table S3	Small specimen: Oumm Qatafa; large specimen: Misliya	2
Mastomys	Molar	m1	2.074	1.75–2.054	Small specimen: [30]: Table 7c; large specimen: [26]: Table S3	Small specimen: Oumm Qatafa; large specimen: Misliya	2
Mastomys	Molar	m1	1.952	1.75–2.054	Small specimen: [30]: Table 7c; large specimen: [26]: Table S3	Small specimen: Oumm Qatafa; large specimen: Misliya	2
Mastomys	Molar	m2	1.432	1.45–1.50	[30]: Table 7c	Oumm Qatafa	2
Mastomys	Molar	m2	1.408	1.45–1.50	[30]: Table 7c	Oumm Qatafa	2
Mastomys	Molar	m3	1.082				
Crocidura[1]	Molar	M1	1.739				
Crocidura	Molar	m1	1.673	1.393–1.536	[26]: Table S3	Misliya	6
Crocidura	Molar	m2	1.635	1.304–1.732	[26]: Table S3	Misliya	11

Crocidura	Molar	m2	1.629	1.304–1.732	[26]: Table S3	Misliya	11
Crocidura	Molar	m1	1.597	1.393–1.536	[26]: Table S3	Misliya	6
Crocidura	Molar	M2	1.499				
Crocidura	Molar	m3	1.451				
Crocidura	Molar	m2	1.18	1.304–1.732	[26]: Table S3	Misliya	11
Crocidura	Molar	m3	1.152				
Arvicanthis	Molar	M1	3.007	3.050–3.200	[30]: Table 6	Oumm Qatafa	2
Arvicanthis	Molar	m2	2.066	1.650–1.850	[30]: Table 6	Oumm Qatafa	3
Arvicanthis	Molar	m3	1.704	1.700–1.750	[30]: Table 6	Oumm Qatafa	2
Apodemus	Molar	m1	1.903	2.250–2.400	[30]: Table 6	Oumm Qatafa	3
[1] The fossil specimens of this genus may contain more than one species.							

Molar tooth length measurements (mm) for Tinshemet specimens, compared to range data available from other regional Lower Paleolithic and early-MP assemblages.

Supplementary Fig. 8: Fossil rodent teeth (*Microtus*) from Tinshemet Cave.

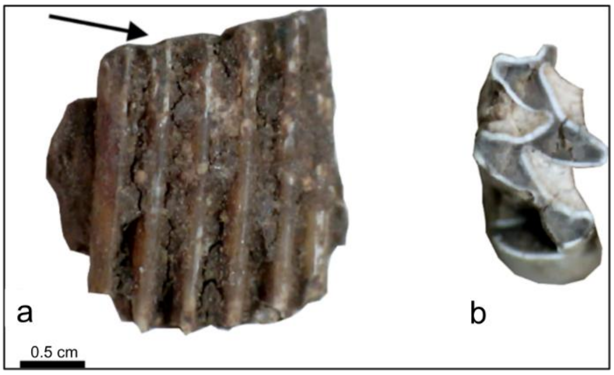

a, Digested tooth, **b**, burned–calcined tooth. Arrow points to the edges of salient angles at the occlusal surface of the tooth, where slight rounding due to light digestion is observed. Scale is 0.5 cm.

S10. Lithic raw materials

The characterization of the raw material is based on the geochemical study of the flint from the nearby site of Nesher Ramla[32]. Tinshemet Cave is found within the same geological settings as Nesher Ramla, with accessibility to the same flint outcrops[33]. Exposures of Mishash Formation flint (Campanian age) are readily available a few kilometres south of Tinshemet Cave. The Mishash flint was the primary type of flint used at the site (Supplementary Fig. 9). The flint types that we considered as “indeterminate” belong to sources that were not identified and are not found in the vicinity of the site. In addition, a large number of the flint artifacts were either too patinated or too burnt to identify their type; thus, their type was considered “indefinable”. The Mishash flint type dominates the assemblages from both the Terrace and First Chamber. The “indeterminate” type of flint occurred at the same frequency in both areas. Due to the higher frequency of burnt and patinated artefacts, “indefinable” flint is more frequent on the Terrace (Supplementary Fig. 9a). The frequencies of raw material types within the main technological categories of lithic artefacts are fairly similar in the two areas (Supplementary Fig. 9b). The "indeterminate” raw material is slightly better represented among the retouched tool and the Levallois flake categories, suggesting a possible import of these end-products to the site.

Supplementary Fig. 9: Raw material exploitation at Tinshemet Cave

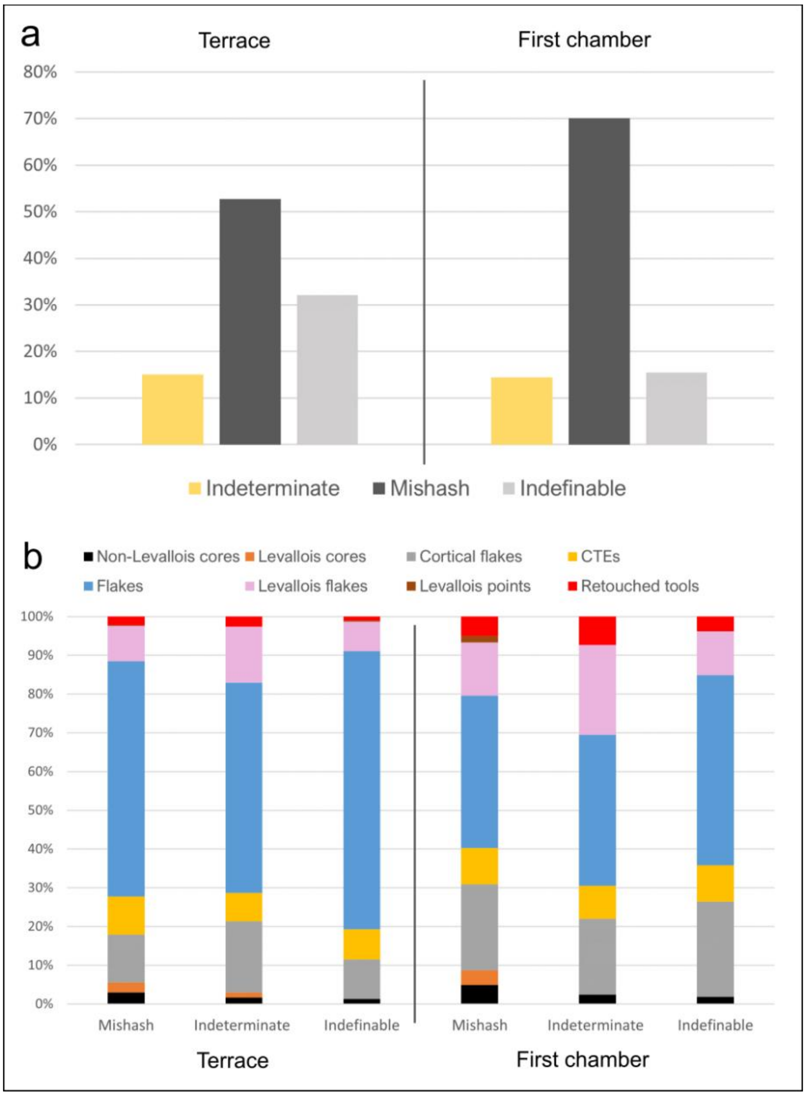

a, Frequency of raw material types in the Terrace and First Chamber. **b**, Main types of lithic artefacts per raw material type and area.

S11. Lithic use-wear analyses

Use-wear analysis was successful in identifying evidence of use on 19 artifacts (Supplementary Table 5, Supplementary Fig. 10). Some artifacts (n= 11) presented a high degree of post-depositional surface modifications (PSDMs), hence not allowing any functional interpretation.

Based on their preservation state, artifacts were assigned to four different categories: **1.** Not altered; **2.** Light alterations; **3.** Medium alterations; **4.** Highly altered. Compromised pieces were either patinated or presented high degrees of post-depositional surface alterations. In some instances, artifacts of the third category did also not allow any functional interpretation (Supplementary Table 5).

Modern surface modifications were observed on some artifacts in the form of metal scratches originated during the excavation activity. Artifacts showing PSDMs were assigned to either the third (medium damage, n=4) or the fourth category (high damage, n=7). Light PSDMs (n=4) did not compromise the functional reading of surfaces. On the rest of the sample (n=29), no PSDMs were observed.

Nineteen artifacts showed some features pointing to use, whereas one artifact was possibly used (Supplementary. Fig. 10a). Thirteen tools did not show any surface modification, suggesting that they were not used. Among the used artifacts, ten showed evidence of transversal movements, six of longitudinal actions (Supplementary Fig. 10b). Transversal movements comprise scraping and whittling actions (Supplementary Fig. 10c), whereas longitudinal movements imply mainly cutting/sawing. Rotational movements were suggested for two artifacts while for one artifact it was not possible to reconstruct the kinematics of the movement due to a lack of linear indicators.

The type of worked material was identified on 18 artifacts. Seventeen tools were used to process hard contact materials (n=17), whereas only one was used in butchery activities (Supplementary Fig. 10d).

Seven tools showed use-wear specific to bone processing, whereas on two artifacts wear pointing to woodworking was documented. The developmental stage of the observed polishes on eight artifacts was not sufficient to distinguish among hard materials (bone, hard wood types).

One artifact (AM19-111-1) showed traces related to the processing of wood while holding the edges at low angles (planing or whittling) (Supplementary Fig. 11). The polish texture is very smooth (Supplementary Fig. 11A: a-d). Wear traces were found on the distal part of both lateral edges, meaning that the two edges were used to perform the same action on wood.

A scraper (AO20-144-7) was found baring traces of a transversal action (i.e., scraping) on hard materials (Supplementary Fig. 11B). The polish is very shiny and polish areas are regularly found along the distal edge. Smaller, shinier, and smoother polished areas were also observed (Supplementary Fig. 11B: a-b). Polished areas are generally very regular and continuous along the edge (Supplementary Fig. 11B: c-d).

Another tool where several used portions where observed is a point (AN20-207-1) displaying an abrupt retouch on both edges (Supplementary Fig. 11C). The right distal edge and the left proximal edge (dorsal view) were used to perform bidirectional movements on a bone (Supplementary Fig. 11C: b, d-e). Isolated shiny polished spots (Supplementary Fig. 11C: a, c) as well as continuous bone polish (Supplementary Fig. 11C: g, h) where observed on such edge portions.

Only two artifacts showed evidence of perforating motions. Use-wear is localized on the retouched portion placed at the convergence of the two lateral edges (tip) on artifact AE26-115-06 (Supplementary Fig. 12). The observed surface modifications can be attributed to a perforating motion on a hard material, possibly bone. Large macro-scars were observed as having a regular distribution on both the portions of the convergent edges, near the pointed extreme (Supplementary Fig. 12A: a-c).

The second artifact displaying evidence of rotational movements is AO19-121-20 (Supplementary Fig. 12B: a). Use-wear is located on the convergence of the two edges. Wear is found on the tip as well as on the distal lateral edges in the form of macro-scars and micro-polish (Supplementary Fig. 12B: b-d). Polish is consistent with experimental evidence on tools used to process bone.

Traces related to butchering activity (i.e. processing of animal muscular tissues) were found on only one artifact (AM19-137-3, Supplementary Fig. 13A: a-b). Relatively well-developed polished areas were observed on this sample, pointing to its use for meat processing activities (Supplementary Fig. 13A: c-e). The tool can be tentatively interpreted as a butchering knife.

Another tool analysed was a lateral scraper on a flake whose proximal lateral edges were probably thinned (AN21-161-2, Supplementary Fig. 13B: a-b). Use-wear connected with a scraping motion on a hard material was found on the distal right edge (dorsal view) (Supplementary Fig. 13B: a). Polished areas are regular and continuous along the edge and are consistent with bone polish (Supplementary Fig. 13B: c-e). There is also suggestive evidence of hafting on this artifact in the form of bright spots (Supplementary Fig. 13B: f-g) and deep striae (Supplementary Fig. 13B: h), probably connected to de-hafting practices. Macro-scars and well-developed polish along the scars pointing to the presence of a haft were also observed (Supplementary Fig. 13B: i-k). Wear connected with hafting was only found on the proximal area of this tool. The hypothesis of this artifact having been used while hafted is coherent with the differential distribution of the two clearly distinguishable wear patterns (use vs. hafting wear) (Supplementary Fig. 13B: a)

Supplementary Table 5: Lithic use-wear features, material type and associated activity.

No.	Reference	Blank	Typology	Position used edge	Macro-use-wear	Striae	Orientation	Polish	Polish type	Movement	Action	Material hardness	Material type	Interpretation	Preservation State
1	AE25-162-1	*débordant* flake	Beak	-	Yes	yes	random	yes	smooth	-	-	-	-	compromised	4
2	AE26-115-6	Levallois flake	Retouched tool	distal	Yes	yes	oblique	yes	smooth	rotational	boring	hard	bone	used	2
3	AO20-144-10	Flake		lat. left	Yes	yes	perpendicular	yes	smooth	transversal	scraping	hard	-	used	1
4	AM19-111-1	Levallois flake	Retouched tool	distal	Yes	no	-	yes	smooth	transversal	whittling	hard	wood	used	1
5	AM20-109-1	Levallois flake		distal	Low	no	-	low	smooth	transversal	scraping	hard	-	used	1
6	AM19-137-3	Levallois flake	Side and end scraper	lat. left	No	no	-	yes	light	longitudinal	cutting	soft	meat	used	1
7	AM21-225-1	Levallois flake		-	No	no	-	no	-	-	-	-	-	not used	1
8	AN21-239-80	Levallois point		distal	Yes	yes	perpendicular	yes	smooth	transversal	scraping	hard	bone	used	1
9	AN20-113-2	*débordant* and overshoot flake		-	Yes	no	-	no						compromised	4
10	AN20-113-4	Pseudo Levallois point		-	No	no	-	no						not used	1
11	AN20-113-3	Levallois flake		left. right	No	no	-	yes	smooth	transversal	scraping	hard	bone/ wood	used	1
12	AN20-231-1			lat. right	No	no	-	yes	smooth	longitudinal	cutting	hard	bone	used	1
13	AN21-129-3	Flake		-	No	no	-	no	-	-	-	-	-	not used	1
14	AN21-120-7	Flake		-	No	no	-	no	-	-	-	-	-	not used	1
15	AN20-108-1	Levallois flake		-	Yes	no	-	no	-	-	-	-	-	not used	1
16	AN20-184-2	Levallois blade		-	Yes	no	-	no	-	-	-	-	-	not used	1
17	AN21-120-4	Levallois flake		-	Yes	yes	random	yes	smooth	-	-	-	-	compromised	3

18	AN21-120-1	Levallois flake		-	No	no		no		-	-	-	-	not used	1
19	AN-21-161-2	Levallois flake	Single convex side scraper	lat. right	Yes	yes	perpendicular	yes	smooth	transversal	scraping	hard	bone	used*	2
20	AN21-161-3	NBK		distal	No	no	-	yes	smooth					possibly used	1
21	AN20-207-5	Levallois flake	Retouched tool	lat. left	No	no	-	yes	smooth	transversal	scraping	hard	bone/ antler	used	1
22	AN20-207-1	Levallois flake	Mousterian point	lat. right and lat.left	Yes	yes	parallel	yes	smooth	longitudinal	cutting	hard	bone	used	2
23	AN20-132-2	Flake		lat. right	No	yes	parallel	yes	smooth	longitudinal	cutting	-	-	used	1
24	AN20-132-1	Broken flake		-	Yes	no	--	yes	smooth	-	-	-	-	compromised	4
25	AN21-238	Broken flake		-	Yes	no		no		-	-	-	-	not used	1
26	AO19-214-1	Levallois point		-	No	no	--	no	-	-	-	-	-	not used	1
27	AO19-110-9	NBK		-	No	no	-	no	-	-	-	-	-	not used	2
28	AO19-110-1	Levallois flake	Single concave scraper	lat. right	Yes	no	-	yes	smooth	transversal	scraping	hard	wood	used	1
29	AO19-121-21	Flake		-	No	no	-	yes	smooth	-	-			not used	1
30	AO20-144-7	Levallois flake	End scraper	distal	No	yes	perpendicular	yes	smooth	transversal	scraping	hard	bone	used	1
31	AO19-121-20	Levallois flake	Retouched tool	-	Yes	no	-	yes	smooth	rotational	boring	hard	bone	used	1
32	AO19-121-23	Blade		-	Yes	no	-	yes	smooth	-	-	-	-	compromised	3
33	AO19-110-7	Flake		-	Yes	no	-	yes		-	-	-	-	compromised	3
34	AO19-110-4	Levallois flake		-	No	no	-	n		-	-	-	-	not used	1
35	AO19-121-26	Levallois blade		-	Yes		-	yes	smooth	-	-	-	-	compromised	4
36	AO19-128-15	Flake	Indeterminate tool	lat. right	Yes	no	-	yes	smooth	-	-	hard	-	used	1
37	AO19-128-1	Levallois flake		lat. left	Yes	yes	-	yes	smooth	transversal	scraping	hard	-	used	1
38	AO19-151-10	Flake		-	Yes	no	-	yes	smooth	-	-	-	-	compromised	4
39	AO19-214-2	Levallois point		-	No	no	-	yes	light	-	-	-	-	compromised	3
40	AO18-180-10	Levallois flake		-	Yes	yes	random	yes	mixed	-	-	-	-	compromised	4

41	AO20-144-6	Levallois flake		-	Yes	no	-	yes	smooth	-	-	-	-	not used	1
42	AO20-144-12	Levallois flake		lat. left	No	yes	parallel	yes	smooth	longitudinal	cutting	hard	bone/antler	used	1
43	AO20-144-8	Flake		-	Yes	yes	random	yes	mixed	-	-	-	-	compromised	4
44	AO20-144-21	Levallois flake		lat. right	No	yes	parallel	yes	smooth	longitudinal	cutting	hard	bone/antler	used	1

Use-wear data on the sample analysed. Position of the used edge, the wear observed, the proposed interpretation, and the preservation state.

Supplementary Fig. 10: Use wear characteristics.

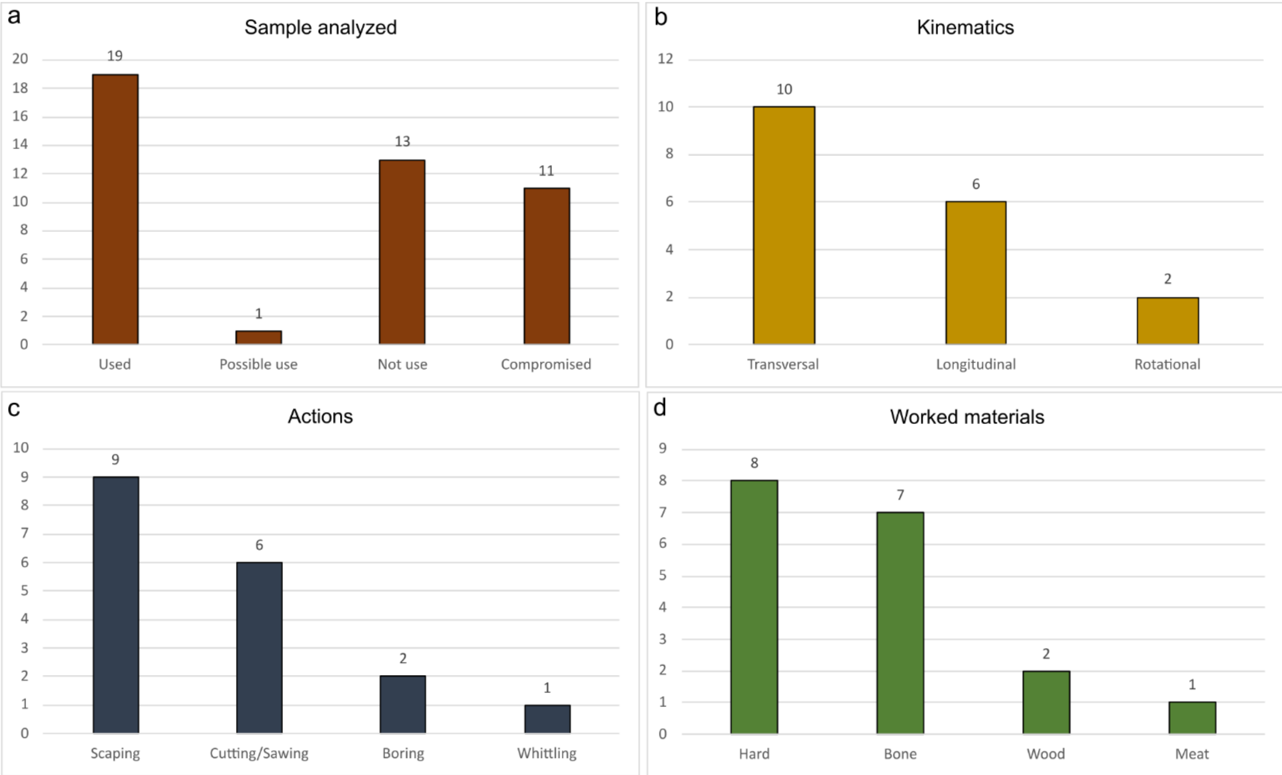

a, the artifacts analysed sorted into interpretative categories based on the presence/absence of wear. **b**, Interpretation of the kinematics of the movements on the artifacts showing use-wear. **c**, the actions performed on the samples analysed. **d**, the worked materials identified on the sample analysed. X-axis=number of artifacts

Supplementary Fig. 11: Use wear features indicating whittling wood, scraping bone and sawing bone.

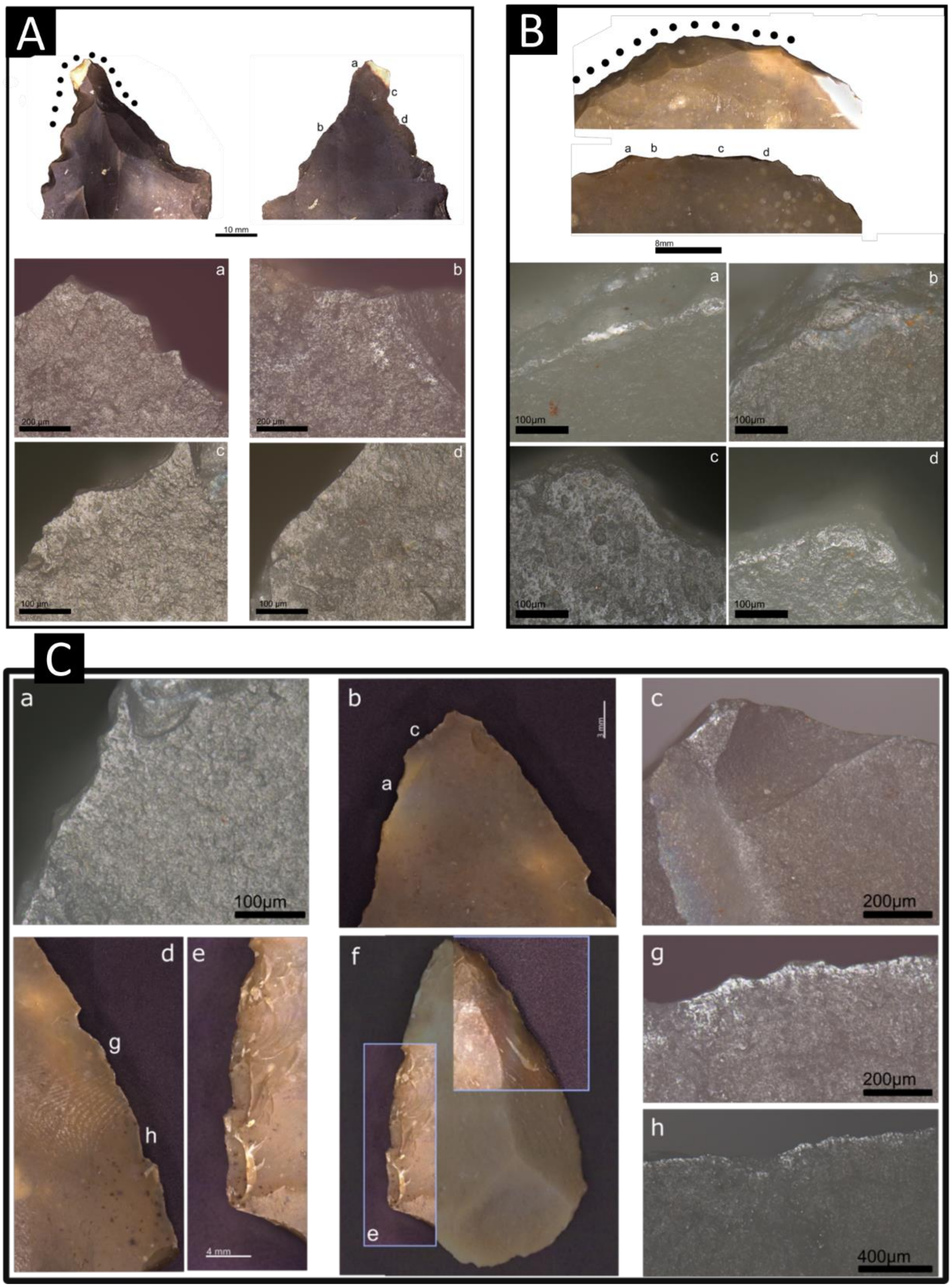

a, Use-wear traces on the artifact AM19-111-1 indicating its use for whittling wood. Dorsal and ventral views of the artifact. Dots indicate the used parts; a-d) Polished areas indicating a transversal action performed at low angles (planning or whittling). **b,** Use-wear traces on the artifact AO20-144-7 indicating its use for scraping bone. a) Dorsal and ventral views of the used portion. Dots indicate the used part; b-e) Bone polish. **c,** Use-wear traces on the artifact AN20-207-1 indicating its use for sawing bone. The small letters represent the localization of the wears on the tool's edge.

Supplementary Fig. 12: Use-wear features indicating perforating bone.

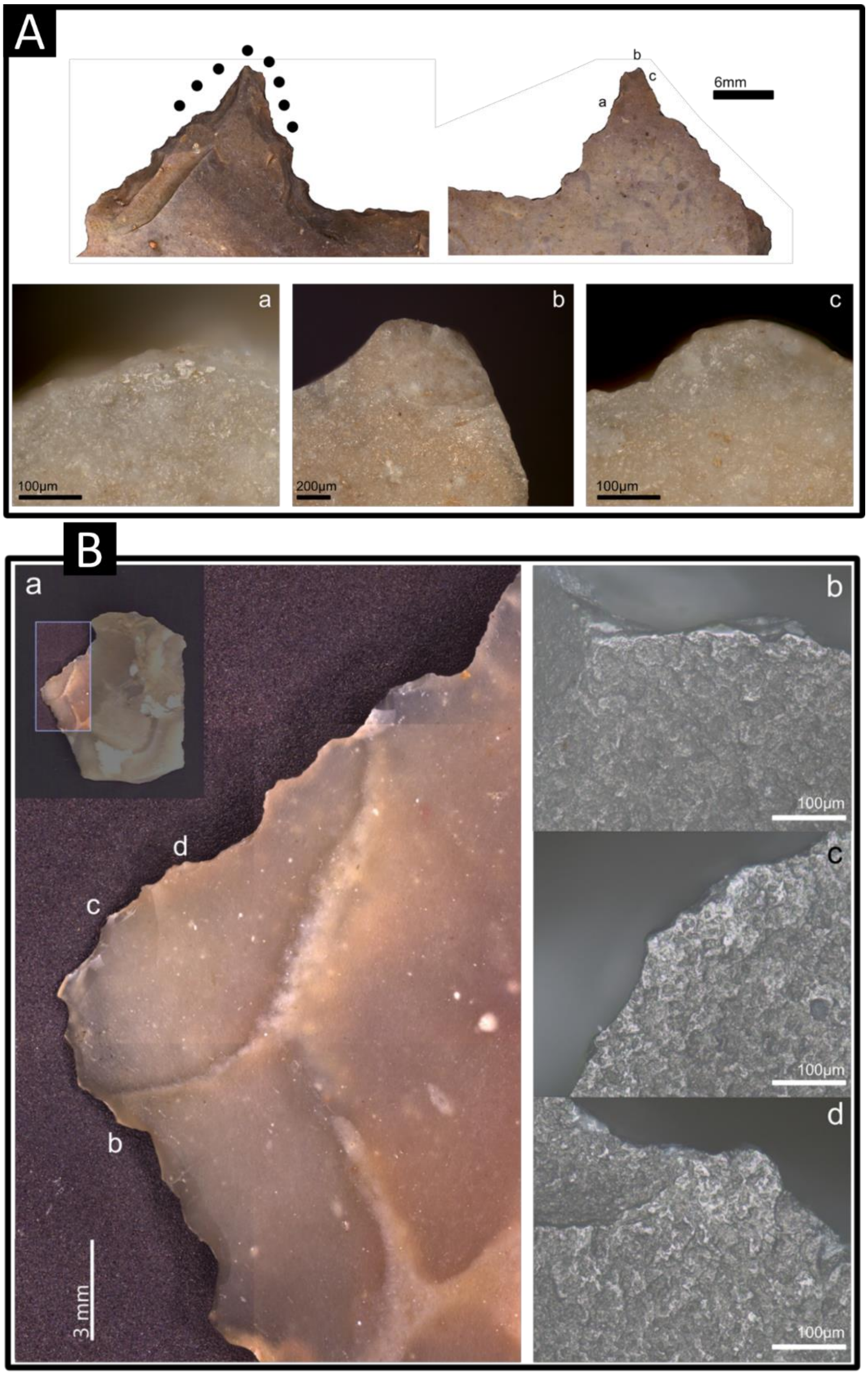

a, Use-wear traces on the artifact AE26-115-06 indicating its use for perforating bone. **b,** Use-wear evidence on AO19-121-20 pointing to its use to perform rotational motions on bone. The small letters represent the localization of the wears on the tool's edge.

Supplementary Fig. 13: Use-wear features indicating meet processing and possible hafting.

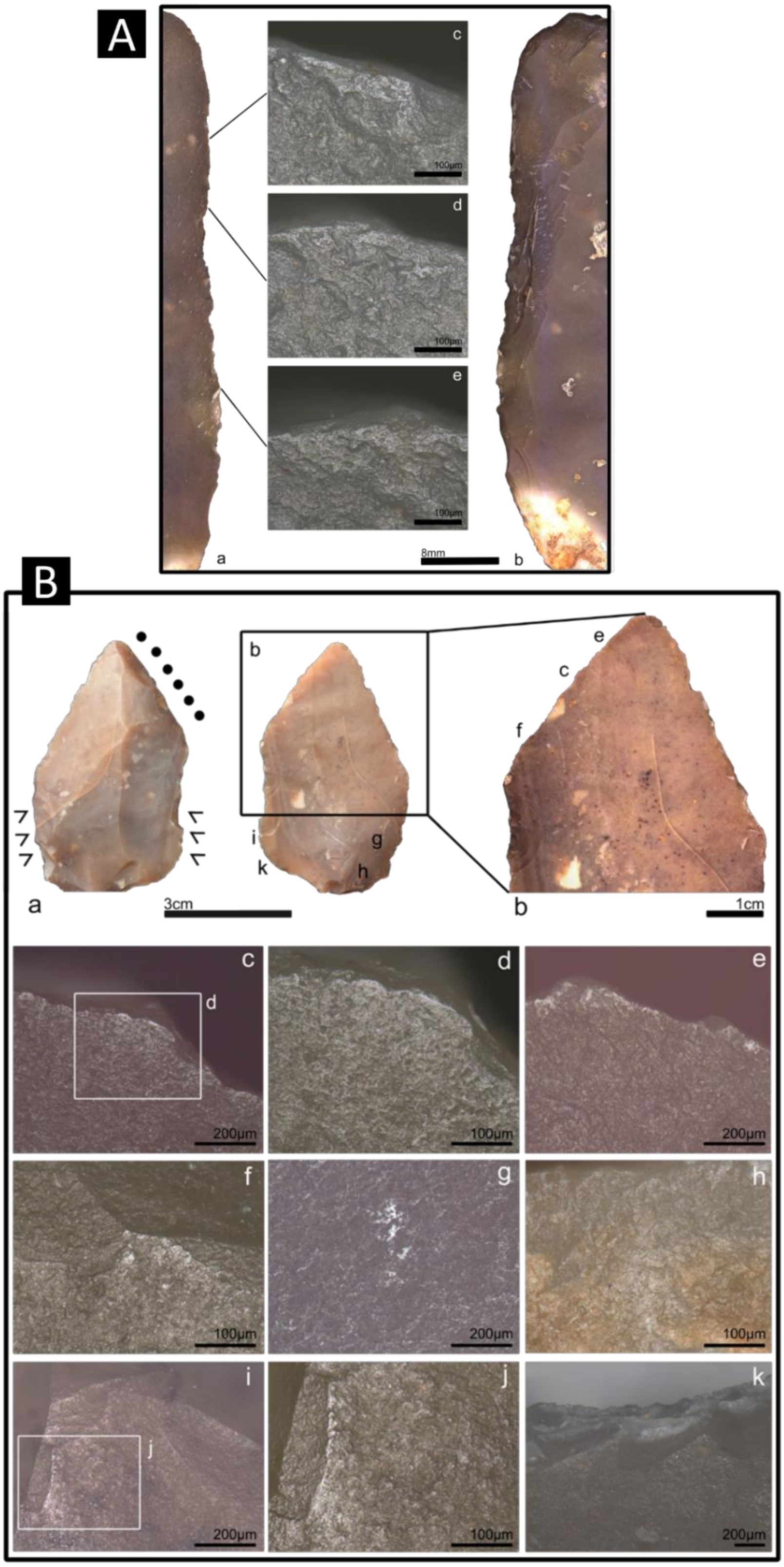

a, Use-wear on AM19-137-3 indicating its use to process meat. **b,** Use-wear (c-e) and traces pointing to hafting (f-k) on artifact AN21-161-2 (a-b). The small letters represent the localization of the wears on the tool's edge.

S12. Ochre

Six different classes of ochre (named I to VI) have been identified microscopically according to grain homogeneity, grain size, texture, compaction of the fabric, and quartz crystals' presence/absence and size (Fig. 4a; Supplementary Fig. 14). These observations, allow us to infer at least four different sources for the ochre provenance. Based on the abundance of quartz, grain size, and texture, classes I and VI are likely related to sandstone deposits. The closest sources of sandstone that bear ochre are 60-80 km away from Tinshemet Cave in northern Samaria and the Lower (southern) Galilee[34]. Classes II and IV are possibly connected to the same provenance rich in iron and quartz and were submitted to higher pressure processes, hence their compaction. Such fine-grained ochre has been previously reported in MP for Skhul, Cave suggesting provenances from Western Samaria and/or the Central Negev Desert[35] (more than 100 km to the south). Class III is from a limestone formation with a very minimal presence of quartz. In some cases, the ochre is still attached to the limestone host rock. Geographically, this type of ochre can be found in closer proximity to Tinshemet Cave than the other sources, with the nearest exposures found in the Samarian Hills (ca. 15-40 km away). The class V ochre derives from oolitic sandstone, which suggests a fourth possible source. Oolitic ochres were defined for some of the materials retrieved from the MP layers of Qafzeh Cave pointing to possible provenances in the Northern Galilee[34] (100 km to the north).

Supplementary Fig. 14: Petrographic slides showing the appearance and identification of ochre classes at Tinshemet Cave.

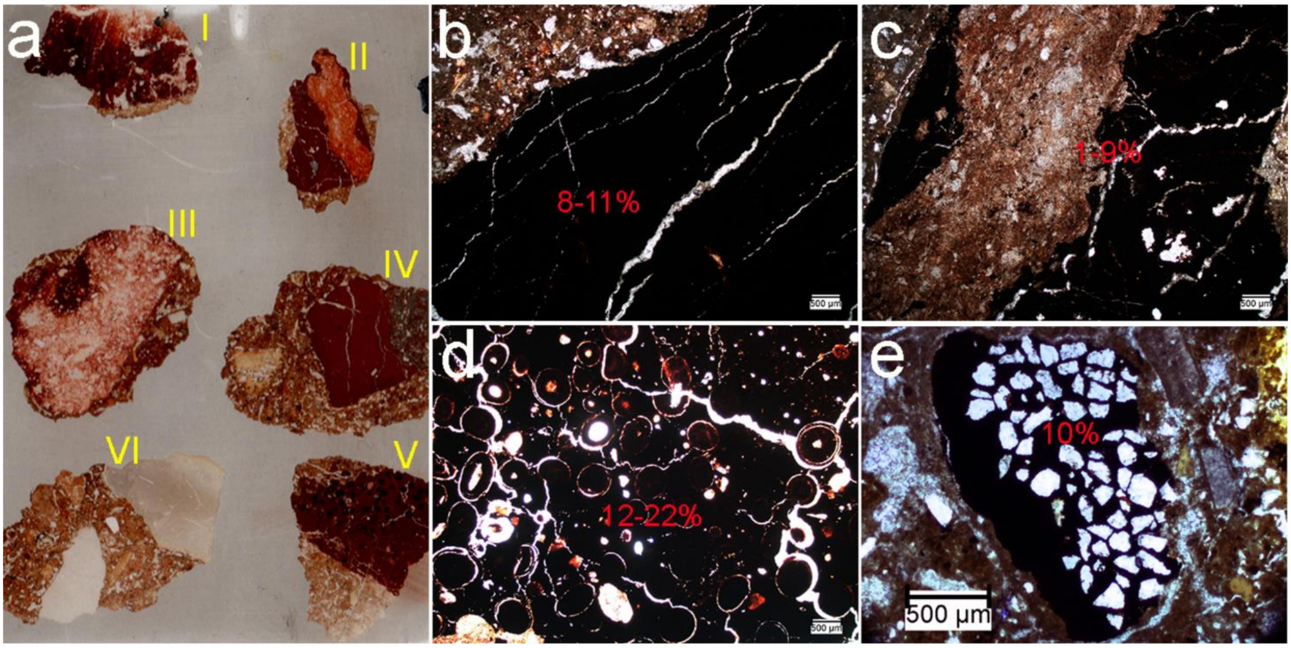

a, Flatbed scan of the thin section containing representative samples of the six ochre classes (I-VI). **b**, Photomicrograph of ochre class IV showing opaque homogenous material with planar voids suggesting ferruginous shale. A similar appearance was also identified in class I. SEM-EDS analysis showed that the atomic content of iron ranges from 8-11% in these samples (n=3). **c**, Photomicrograph of ochre class III (also identified in class II) showing red-brown coloured limestone surrounded by opaque ochre. The lower iron atomic content (1-9%; n=4) in classes II and III, relative to classes I and IV, reflects the 'dilution' of iron due to the presence of calcite from limestone. **d**, Photomicrograph of ochre class V showing opaque ochre composed of oolites. The iron atomic content range in this sample is 12-22% (n=2). **e**, Photomicrograph showing an example of sandstone ochre. This example contains coarse sand-sized angular quartz grains within an iron oxide matrix. The iron atomic content in this sample is 10% (n=1). All photomicrographs were taken using plane polarized light.

S13. Faunal assemblages

The Tinshemet Cave excavation yielded abundant faunal material in very variable degrees of preservation. Generally, faunal remains from the Inner Chamber of the cave are well preserved. However, they become more degraded on the Terrace, especially in the uppermost cemented sediments. In the latter context, bone cortical surfaces are sometimes absent, and bone extraction from the hard breccia is generally challenging. For this report, we studied the skeletal elements readily identifiable at the genus or species level, i.e., teeth, epiphyses, phalanges, carpals, and tarsals, from a portion of the excavated material in the field. Numerous identifiable bone fragments that can be identified to size-class remain in the bags and will be incorporated in the ensuing detailed analysis (Extended Data Table 5).

Most MP fauna in the southern Levant are known from the Mt. Carmel-Galilee region further to the north. The cave sites are typically dominated by two ungulate species, mountain gazelle and Mesopotamian fallow deer, with some contribution of aurochs and usually small numbers of red deer. Wild boar, caprines, and equids are generally rare. The anthropogenic assemblages are usually dominated by the small-bodied gazelle, while natural accumulations (carnivore dens or natural pitfall traps) are dominated by medium-sized ungulates, especially fallow deer ([36] and references therein). Recently, two MP cave sites near Tinshemet Cave yielded faunal assemblages: an anthropogenic deposition in Emanuel Cave[37] and a natural pitfall trap at Rantis Cave[4], conforming to this pattern. Another sizeable faunal assemblage in the cave's vicinity is the late Lower Palaeolithic Qesem Cave, where fallow deer dominate alongside some aurochs, equids, and red deer; gazelle are virtually absent[38]. Aside from caves, the open-air MP sequence of Nesher Ramla in the vicinity of Tinshemet Cave also yielded rich faunas deposited in the context of a karstic depression. Unit III of Nesher Ramla is dominated by aurochs, alongside numerous tortoise remains[39].

Against this backdrop, the Tinshemet faunal composition indicates a similar mosaic of taxa from open and wooded Mediterranean settings, but it is more even (four ungulate species in similar proportions) and richer in larger ungulates than other MP cave archaeofaunas in the Levant. Among cave sites, the mid-MP Skhul Cave shows a similarly large proportion[40], although this assemblage is probably biased due to the selective collection of larger bones. Only open-air sites display higher proportions of large ungulates, as observed in the nearby mid-MP Nesher Ramla site (e.g., Unit III;[39]). It is tempting to speculate that the specialized mortuary activity that had occurred in the cave impacted the archaeofaunal pattern, for example, as a stronger focus on consuming the largest animals in the landscape, which could also be the case at Qafzeh and Skhul caves (see below; e.g., in a much later context[41]). On the other hand, cemented deposits are known to bias assemblage composition in favor of large-bodied taxa[42–44]. Nevertheless, the cave site of Emanuel demonstrates a much lower proportion of *Bos* and *Equus,* despite having been extracted from cemented sediments[37].

S14. Middle Palaeolithic chrono-cultural framework of the Levant

The Early Middle Palaeolithic. The EMP is dated to ca. 250-150 ka ago[45–47] (Supplementary Table 6). The lithic assemblages of the EMP sites exhibit several common characteristics, suggesting that they represent a single technological entity[48–54]. These include a combination of the Levallois and laminar technologies for producing elongated Levallois points, as well as triangular flakes and blades retouched into various types of points[49–51,55]. Blades and elongated points represent the major group of blanks in the EMP assemblages (about 30% in the Misliya and Hayonim Caves and 50% in Unit IX in Tabun Cave[54]). The blades were produced by semi-rotating or rotating unidirectional or bidirectional methods[48–51,54]. The Levallois flakes are mostly elongated, with triangular and subtriangular shapes and convergent scar patterns. Bi-directional preparation of Levallois cores is also present[48,55], whereas centripetal Levallois flakes are very rare (Fig. 6a; Supplementary Table 7). Given that a small number of flakes with a centripetal scar pattern could be a random product of any reduction sequence and not necessarily a result of the centripetal Levallois method, their presence in low numbers at EMP sites cannot be taken as an unequivocal indicator for the use of the centripetal Levallois method. Centripetal Levallois cores and *débordant* flakes, which represent centripetal Levallois core preparation, are also virtually absent[48]. The rare occurrence of centripetal Levallois cores, blanks, and core maintenance products suggests that the centripetal Levallois reduction strategy was either not employed, or very rarely employed during EMP. The EMP industry disappeared from the Levantine archaeological record during the second half of MIS 6, ca. 160-140 ka ago.

The mid-Middle Palaeolithic. The second cluster of Levantine MP sites, among them Tinshemet Cave, is dated to MIS 5 (Supplementary Table 6). Regarding lithic technology and typology, these sites fundamentally differ from the preceding EMP[48,56–59]. The MIS 5 sites are dominated by centripetal Levallois technology and the Levallois blanks are dominated by items with centripetal scar patterns (Fig. 6a; Extended Data Table 4; Supplementary Table 7). The centripetal industries were reported from Tabun Layer C, Skhul, Naamé, Nahr Ibrahim, and Ras el-Kelb[58,60–64]; however, they are described in detail only at Qafzeh Cave and Nesher Ramla[57,65–67]. Nesher Ramla, Qafzeh, Skhul, Tabun (Layer C), Nahr Ibrahim, and Naamé (dating the *Strombus* and *Vermetes* layer underlying the Mousterian occupations) provided absolute age estimations, all falling within MIS 5[40,60–64,68,69] (Supplementary Table 6). This cluster of sites in the Levant is associated with the *H. sapiens* fossils discovered at Qafzeh and Skhul Caves[70–72] and the pre-Neanderthal fossils at Nesher Ramla[73]. In addition, in the adjacent northwestern Arabian Peninsula, a cluster of sites with centripetal Levallois industries was recently discovered[74–78]. Most of these sites are surface collections attributed to MIS 5, according to their environmental context. However, some provide absolute dates, all within MIS 5. At one of these sites, Al-Wusta, a human phalanx attributed to *H. sapiens* was discovered[74].

Supplementary Table 6: Chronology of the early Middle Palaeolithic and mid-Middle Palaeolithic sites in the Levant.

Chrono-cultural period	Site	Chronology	Human remains
Early MP	Hayonim Cave[46]	210 ± 28 ka	
		221 ± 21 ka	
	Hummal[79]	190 ± 35 ka	
		210±40ka	
	Misliya Cave[47]	250-160 ka	x
	Emmanuel Cave[37]	191±1 Ka	
	Tabun Cave IX[45]	256 ± 26 ka	
Mid-MP	Qafzeh Cave[57,80]	115-90 ka	x
	Skhul Cave Layer B[40,60,61,81]	130-100 ka	x
	Tabun Cave Layer C[40,45,82]	190-150 ka;	x
	Ras el-Kelb[64]	160-105 ka	x
		>52 ka	
	Naamé[62]	90±20 ka	
	Nahr Ibrahim Cave[83]	ca. 92-80 ka	
	Nesher Ramla[65,84]	126 ± 6 ka 176± 52- 94±18 ka	x
	Tinshemet Cave	*this paper*	x

Dates of the main Levantine early and mid-MP sites mentioned in the text, and the presence of human remains.

Nesher Ramla and Qafzeh Cave provide large and stratified lithic assemblages that were subjected to a detailed technological study[57,65–67]. These studies suggest that throughout the MP sequence of both sites, the centripetal Levallois method was the major production system. Levallois products include centripetal Levallois cores, oval and quadrangular flakes with facetted striking platforms, *débordant* flakes, pseudo-Levallois flakes, and pseudo-Levallois points[65–67]. A detailed comparison between Qafzeh Cave and Nesher Ramla revealed many technological similarities[65]. The resemblance lies in the fine details, such as the technological details of the core preparation and their exploitation. Although other Levantine and Arabian centripetal Levallois assemblages were only partially reported or are represented by small assemblages, they show a similar picture. The Skhul, Naamé, Hummal, Nahr Ibrahim, Tabun Layer C, and Arabian sites show the presence of the characteristic centripetal Levallois maintenance products, centripetal Levallois cores, and oval Levallois flakes[60–63,74,78,85,86].

An additional common feature of the MIS 5 industries in the Levant and northwestern Arabia is the occurrence of the Levallois points produced by a unidirectional convergent method (reported from Qafzeh, Skhul, Naamé, Nesher Ramla, and JKF1[87]). In both Qafzeh and Nesher Ramla, the preferential method is the most common one used for the production of flat Levallois points. In both sites, most of the Levallois cores for points' production exhibit a single preferential scar in the center of the core debitage surface. The Levallois points exhibit mostly a unidirectional convergent scar pattern. They are flat and symmetrical with straight or slightly convex profiles[57,65]. This pattern is confirmed by recent studies at Skhul Cave, where most points were produced by a unidirectional convergent method[60,61]. The points at Skhul Cave were primarily produced by preferential Levallois reduction[60]. The Levallois points occur in shifting frequencies, sometimes in low numbers, as in Unit III of Nesher Ramla, Tinshemet Cave, some layers of Qafzeh and several other sites. In other cases, they are frequent, as in Unit VI of Nesher Ramla, Layers XIV and XV in Qafzeh[57], and possibly also in Skhul Cave[60,61] (Supplementary Fig. 15).

The main differences between the MIS 5 sites are evident in the frequencies of the retouched tools, Levallois points, and cortical pieces, and the shifts in the importance of different knapping systems (the centripetal method vs. the Levallois convergent unidirectional point production methods). These differences occur both at the inter- and intra – site level. An additional difference is the use of the lateral tranchet blow (LTB) technique, which was only recorded at Nesher Ramla[88,89]. Except for the latter, the differences are not qualitative and may be due to local circumstances. For example, raw materials are readily available in the Nesher Ramla vicinity, whereas flint is not available at Qafzeh Cave in the immediate surroundings. In terms of site function, Nesher Ramla is interpreted as a camp linked to hunting and animal butchering, whereas Qafzeh Cave served as a burial ground (Layers XXII-XV) or as a short-term habitation locality (Layers XV-V). Thus, the differences in the frequencies of different technological and typological groups are likely to be linked to differences in site function, changes in the mobility pattern and the length of the occupation, and the distances to raw material sources rather than to major differences in the core reduction systems. Nonetheless, some stylistic and cultural differences on a local scale do occur, such as the use of the LTB technique for tool production and maintenance at Nesher Ramla[88].

Supplementary Fig. 15: Frequencies of the Levallois points among Levallois products in mid-Middle Palaeolithic sites.

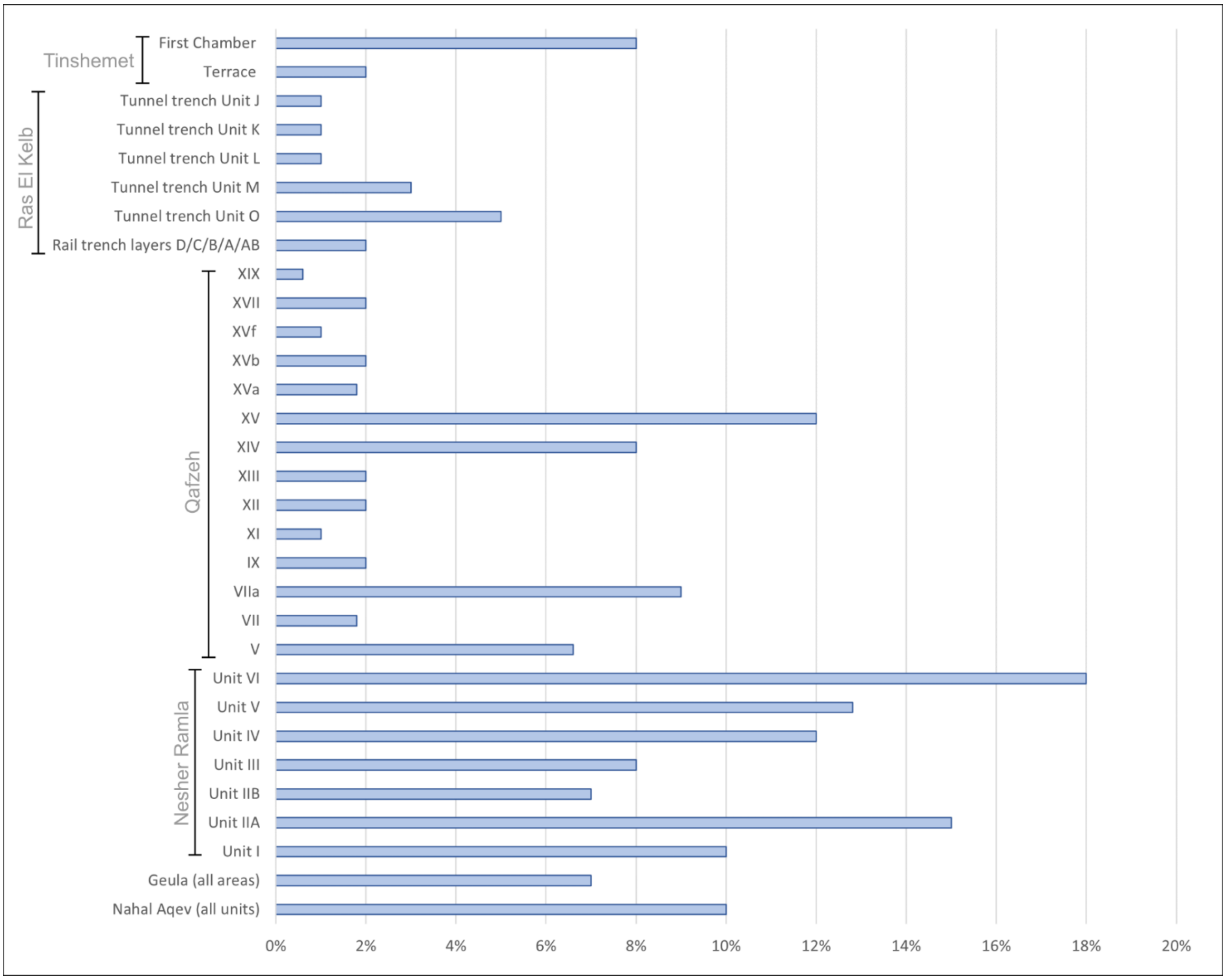

Frequency of the Levallois points among the total amount of Levallois blanks in the mid-MP sites in the Levant.

Supplementary Table 7: Frequencies of centripetal Levallois flakes among Levallois products in the Levantine Middle Palaeolithic sites.

	Site	Centripetal Levallois flake	
Late-MP	**Kebara***[90]	%	N
	unit VI	28.6%	340
	unit VII	31.0%	493
	unit VIII	28.80%	219
	unit IX	21.20%	554
	unit X	24.80%	534
	unit XI	19.10%	487
	unit XII	13.70%	175
	Amud[91]		
	B1	<20.0%	283 (excl. Ret)
	B2	ca. 30%	362
	B4	ca. 30%	86
	Tor Faraj (floor I-II)[92]	2.0%	414
	Umm El Tlel**[93]		
	v2 βa	2.70%	602
	v2 γ/Δa	2.60%	342
	v2 Δa np.	1.40%	139
	v2 Δa p.	28.20%	312
	v2 πa	12.0%	92
	v2 πb	3.60%	471
	Yabrud I**[93]		
	layer 2	6.50%	278
	layer 3	6.90%	405
	layer 4	2.10%	563
	layer 5	28.0%	471
	layer 6	8.0%	313
Mid-MP	**Nahal Aqev (all units)****[21]	>40.0%	691
	Nesher Ramla*[65–67]		
	Unit I	46.20%	200 (excl. Ret)
	Unit IIA	51.60%	119
	Unit IIB	54.00%	1047
	Unit III	67.00%	872
	Unit IV	54.80%	286
	Unit V	49.50%	445
	Unit VI	64.80%	166
	Geula (all areas)*[94]	36.0%	182
	Qafzeh*[57]		
	V	43.70%	71

	VIIa	40.30%	79
	IX	46.10%	202
	XI	66.70%	146
	XII	66.60%	82
	XIII	71.90%	306
	XIV	59.40%	95
	XV	36.60%	1117
	XVa	60.00%	193
	XVf	50.60%	203
	XVII	71.60%	193
	XIX	77.90%	125
	XXI	67.20%	88
	Ras el Kelb* [64]		
	Rail trench layers D/C/B/A/AB	59.0%	802
	Tunnel trench Unit O	64.50%	177
	Tunnel trench Unit N	77.30%	160
	Tunnel trench Unit M	50.0%	291
	Tunnel trench Unit L	67.10%	855
	Tunnel trench Unit K	71.40%	950
	Tunnel trench Unit J	70.90%	1461
	Tinshemet*		
	Terrace	61.0%	79
	First Chamber	75.0%	59
Early-MP	**Tabun IX** [54]	3.10%	219
	Misliya Unit 5-6c* [48]	3.40%	541
	Hayonim F (unit 10/9/7-8)** [52]	6.30-9.30%	4186
	Emanuel Cave (all units)** (Goder-Goldberger pers.comm)	9.20%	76
	Hummal 6b** [95]	9.0%	99

*Among Levallois flakes

** Among Levallois blanks (flakes, points, and blades)

Note: only layers with more than 50 Levallois blanks are included.

S15. Use of ochre in the Levantine Middle Palaeolithic

Ochre has been found in the Levantine MP sites dating to MIS 5 only (Supplementary Table 8). In addition to Tinshemet Cave, ochre is reported in cave sites such as Skhul[35,96], Qafzeh,[34,97,98] Nahr Ibrahim[99], as well as in the open-air site of Nesher Ramla[84,100].

At Skhul Cave, Mount Carmel, four ochre chunks with colours from red to orange are reported from the hard-cemented Unit B2. The chunks are between 1 and 3 cm in size, whereas additional millimetric fragments embedded in samples of the hard sediment are also preserved[96]. Three of the pieces were suggested to have been intentionally heated. The ochre was obtained from different sources located at distances up to 80 km from the site[35,96].

Qafzeh Cave, Lower Galilee, Israel, presents a collection of 84 ochre pieces throughout Layers XXIV-XVII of the site, from which 71 pieces were studied[34]. The colours of most of the pieces vary from red to pink, with a few being yellow to brown hues (5%). The assemblage presents a wide variability in petrological terms, suggesting provenance from multiple sources. At least two ochre pieces underwent thermal alteration[98]. Another ochre piece presents scraping marks and concavities on its facets, and eleven lithic artefacts show remains of ochre[34]. Additionally, several seashells recovered from the lowermost layers of the site bear ochre stains[97]. At Qafzeh, the ochre was found both in and outside burial contexts[34,101].

At Nahr Ibrahim Cave, Lebanon, dispersed fragments of red ochre were reported in the context of a concentration of deer bones with no indication of consumption. This was interpreted as a ritual animal burial event that included the use of mineral red pigment[99].

Finally, at the open-air site of Nesher Ramla, Israel, a collection of 208 ochre pieces was retrieved from Units VI-I, along the entire eight-meters-long sequence[84,100]. The material is diverse in its fabric, texture, and grain size.

Supplementary Table 8: Presence of ochre in the Levantine Middle Palaeolithic sites.

Chrono-cultural period	Use of ochre
Early MP	No ochre use reported
Mid-MP	Evidence at Qafzeh, Skhul, Nahr Ibrahim, Nesher Ramla, and Tinshemet[34,35,84,96–99]
Late-MP	No ochre use reported

Exploitation of pigment (ochre) in the three chrono-cultural phases of the Levantine MP.

S16. Faunal assemblages in the Levantine Middle Palaeolithic

Most MP faunas in the southern Levant are known from the Mt. Carmel-Galilee region further north of Tinshemet Cave. The cave sites are typically dominated by two ungulate species, mountain gazelle (*Gazella gazella*) and Mesopotamian fallow deer (*Dama mesopotamica*), with some contribution of aurochs (*Bos primigenius*) and small numbers of other cervids and bovids. This is especially true for the EMP sites, in which gazelle and fallow deer represent 72–83% of the assemblages (Supplementary Table 9; Fig. 6b). The mid-MP faunal composition is more even and is richer in larger ungulates than the EMP and late MP cave archaeofaunas in the Levant. The proportion of the largest ungulate taxa, mostly aurochs and occasionally equids, hippopotamus, and rhinoceros, in the MIS 7-6 caves of Misliya[102], Hayonim[103], Tabun Layer D[44], and Emanuel[37], and MIS 4/3 sites of Kebara[104], Amud[105], and Shovakh[106] is consistently lower than that of the MIS 5 caves of Qafzeh[107], Tabun Layer C[44], and Tinshemet (Fig. 6b; Supplementary Table 9). The mid-MP Skhul Cave shows a similarly large proportion[40], although this assemblage is probably biased due to the selective collection of larger bones and therefore it was not included in Supplementary Table 9. Aside from caves, this pattern is repeated at the open-air mid-MP sequence of Nesher Ramla, which yielded rich faunas dominated by aurochs and numerous tortoise remains[39].

Supplementary Table 9: Ungulate abundance (based on NISP) in Middle Palaeolithic Levantine cave-sites

	Early				Middle			Late		
	Misliya[102]	Hayonim lower E[103]	Emanuel[37]	Tabun D[44]	Tabun C[44]	Qafzeh[107]	Tinshemet	Shovakh[106]	Amud[105]	Kebara[104]
Gazella	171	1567	49	187	187	91	46	27	291	4573
Dama	131	988	24	141	43	193	33	5	60	2507
Capra	8	3	0	6	15	97	7	4	18	74
Cervus	6	120	7	46	21	198	3	0	5	968
Sus	14	151	0	13	38	62	4	1	17	400
Bos	32	235	21	31	100	171	47	2	1	2030
Capreolus	1	3	1	5	0	5	0	0	1	20
*Equus***	0	17	0	3	15	78	27	0	0	133
Rhinocerotidae	0	1	0	12	26	35	1	0	1	17
Alcelaphus	0	0	0	0	0	7	0	0	0	12
Hippopotamus	0	0	0	7	35	0	0	0	0	0
Camelus	0	0	0	0	0	0	0	0	0	0
Total	**363**	**3085**	**102**	**451**	**480**	**937**	**168**	**39**	**394**	**10734**

Note: only cave assemblages that result from human activities were included.

References:

1. Stekelis, M. Preliminary Report on Soundings in Prehistoric Caves in Palestine. *American Schools of Oriental Research* 2–10 (1942).
2. Frumkin, A., Langford, B., Marder, O. & Ullman, M. Paleolithic caves and hillslope processes in south-western Samaria, Israel: Environmental and archaeological implications. *Quaternary International* **398**, 246–258 (2015).
3. Frumkin, A. & Fischhendler, I. Morphometry and distribution of isolated caves as a guide for phreatic and confined paleohydrological conditions. *Geomorphology* **67**, 457–471 (2005).
4. Marder, O. *et al.* Mammal remains at Rantis Cave, Israel, and Middle–Late Pleistocene human subsistence and ecology in the Southern Levant. *Journal of Quaternary Science* **26**, 769–780 (2011).
5. Raviv, D., Sasson, S. T., Langford, B., Frumkin, A. & Zissu, B. An Archaeological Survey at Naḥal Bet ʻArif Cave, Israel. *Zeitschrift des Deutschen Palästina-Vereins* (Forthcoming).
6. Shahack-Gross, R., Berna, F., Karkanas, P. & Weiner, S. Bat guano and preservation of archaeological remains in cave sites. *Journal of Archaeological Science* **31**, 1259–1272 (2004).
7. Gur-Arieh, S., Mintz, E., Boaretto, E. & Shahack-Gross, R. An ethnoarchaeological study of cooking installations in rural Uzbekistan: development of a new method for identification of fuel sources. *Journal of Archaeological Science* **40**, 4331–4347 (2013).
8. Cabanes, D., Weiner, S. & Shahack-Gross, R. Stability of phytoliths in the archaeological record: a dissolution study of modern and fossil phytoliths. *Journal of Archaeological Science* **38**, 2480–2490 (2011).
9. Karkanas, P. *et al.* Evidence for habitual use of fire at the end of the Lower Paleolithic: Site-formation processes at Qesem Cave, Israel. *Journal of Human Evolution* **53**, 197–212 (2007).
10. Ogloblin Ramirez, I., Dunseth, Z. C., Shalem, D. & Shahack-Gross, R. Infrared spectra of mixtures of heated and unheated clay: Solving an interpretational conundrum. *Geoarchaeology* (2023) doi:10.1002/gea.21976.

11. Carrión, J. S., Scott, L. & Marais, E. Environmental implications of pollen spectra in bat droppings from southeastern Spain and potential for palaeoenvironmental reconstructions. *Review of Palaeobotany and Palynology* **140**, 175–186 (2006).
12. Leroy, S. A. G. & Simms, M. J. Iron age to medieval entomogamous vegetation and Rhinolophus hipposideros roost in South-Eastern Wales (UK). *Palaeogeography, Palaeoclimatology, Palaeoecology* **237**, 4–18 (2006).
13. Marais, E., Scott, L., Gil-Romera, G. & Carrión, J. S. The potential of palynology in fossil bat-dung from Arnhem Cave, Namibia. *Transactions of the Royal Society of South Africa* **70**, 109–115 (2015).
14. McCobb, L. M. E., Briggs, D. E. G., Evershed, R. P., Hall, A. R. & Hall, R. A. Preservation of Fossil Seeds From a 10th Century AD Cess Pit at Coppergate, York. *Journal of Archaeological Science* **28**, 929–940 (2001).
15. Langgut, D. *et al.* Micro-archaeological indicators for identifying ancient cess deposits: An example from Late Bronze Age Megiddo, Israel. *Journal of Archaeological Science: Reports* **9**, 375–385 (2016).
16. Dunseth, Z. C. *et al.* Archaeobotanical proxies and archaeological interpretation: A comparative study of phytoliths, pollen and seeds in dung pellets and refuse deposits at Early Islamic Shivta, Negev, Israel. *Quaternary Science Reviews* **211**, 166–185 (2019).
17. Herrera, L. G. & Martínez Del Río, C. Pollen Digestion by New World Bats: Effects of Processing Time and Feeding Habits. *Ecology* **79**, 2828–2838 (1998).
18. Maher, L. J. Environmental information from guano palynology of insectivorous bats of the central part of the United States of America. *Palaeogeography, Palaeoclimatology, Palaeoecology* **237**, 19–31 (2006).
19. Coles, G. M. & Gilbertson, D. D. The Airfall-pollen Budget of Archaeologically Important Caves: Creswell Crags, England. *Journal of Archaeological Science* **21**, 735–755 (1994).
20. Pendleton, M. W., Bryant, V. M. & Pendleton, B. B. Entomopalynology. in *Palynology: Principles and Applications* (eds. Jansonius, J. & McGregor, D. C.) 239–243 (Foundation, Dallas, 1996).

21. Barzilai, O. *et al.* Expansion of Eastern Mediterranean Middle Paleolithic into the Desert Region in early Marine Isotopic Stage 5. *Nature Scientific Reports* (2022).
22. Satow, C. *et al.* Detection and Characterisation of Eemian Marine Tephra Layers within the Sapropel S5 Sediments of the Aegean and Levantine Seas. *Quaternary* **3**, 6 (2020).
23. Zhang, S. *et al.* Distal tephra reveal new MIS 5e Kos eruptions: Implications for the chronology and volcanic evolution histories in the Eastern Mediterranean region. *Quaternary Science Reviews* **307**, 108054 (2023).
24. Rabinovich, R. & Tchernov, E. Chronological, paleoecological and taphonomical aspects of the Middle Paleolithic site of Qafzeh, Israel. in *Archaeozoology of the Near East II* (eds. Buitenhuis, H. & Uerpmann, H.-P.) 5–44 (Backhuys Publisher, Leiden, 1995).
25. Tchernov, E. The faunal sequence of the southwest Asian Middle Paleolithic in relation to hominid dispersal events. in *Neandertals and Modern Humans in Western Asia* (eds. Akazawa, T., Aoki, K. & Bar-Yosef, O.) 77–90 (Plenum Press, New York, 1998).
26. Weissbrod, L. & Weinstein-Evron, M. Climate variability in early expansions of Homo sapiens in light of the new record of micromammals in Misliya Cave, Israel. *Journal of Human Evolution* **139**, 102741 (2020).
27. Jelinek, A. J., Farrand, W. R., Haas, G., Horowitz, A. & Goldberg, P. New excavations at the Tabun Cave, Mount Carmel, Israel, 1967-1972: A preliminary report. *Paléorient* **1**, 151–183 (1973).
28. Belmaker, M. & Hovers, E. Ecological change and the extinction of the Levantine Neanderthals: implications from a diachronic study of micromammals from Amud Cave, Israel. *Quaternary Science Reviews* **30**, 3196–3209 (2011).
29. Maul, L. C. *et al.* Microfaunal remains at Middle Pleistocene Qesem Cave, Israel: Preliminary results on small vertebrates, environment and biostratigraphy. *Journal of Human Evolution* **60**, 464–480 (2011).
30. Tchernov, E. *Succession of Rodent Faunas during the Upper Pleistocene of Israel*. (Paul Parey: Hamburg & Berlin., 1968).

31. Weissbrod, L., Dayan, T., Kaufman, D. & Weinstein-Evron, M. Micromammal taphonomy of el-Wad Terrace, Mount Carmel, Israel: distinguishing cultural from natural depositional agents in the Late Natufian. *Journal of Archaeological Science* **32**, 1–17 (2005).

32. Ekshtain, R. & Zaidner, Y. Raw material exploitation at the Middle Paleolithic site of Nesher Ramla, Israel. *Quaternary International* (2021) doi:10.1016/j.quaint.2021.02.038.

33. Yechieli, Y. Geological map of Israel 1:50,000 Sheet 8-III Lod. Jerusalem. *Geological Survey of Israel* (2008).

34. Hovers, E., Ilani, S., Bar-Yosef, O. & Vandermeersch, B. An Early Case of Color Symbolism: Ochre Use by Modern Humans in Qafzeh Cave. *Current Anthropology* **44**, 491–522 (2003).

35. Salomon, H. *et al.* Selection and heating of colouring materials in the Mousterian level of Es-Skhul (c. 100 000 years BP, Mount Carmel, Israel). *Archaeometry* **54**, 698–722 (2012).

36. Yeshurun, R. Middle Paleolithic Prey Choice Inferred from a Natural Pitfall Trap: Rantis Cave, Israel. in *Zooarchaeology and Modern Human Origins: Human Hunting Behavior during the Later Pleistocene* (eds. Clark, J. L. & Speth, J. D.) 45–58 (Springer Netherlands, Dordrecht, 2013). doi:10.1007/978-94-007-6766-9_4.

37. Goder-Goldberger, M. *et al.* Emanuel Cave: the site and its bearing on early Middle Paleolithic technological variability. *Paléorient* **38**, 203–225 (2012).

38. Blasco, R., Rosell, J., Gopher, A. & Barkai, R. Subsistence economy and social life: A zooarchaeological view from the 300kya central hearth at Qesem Cave, Israel. *Journal of Anthropological Archaeology* **35**, 248–268 (2014).

39. Crater Gershtein, K. M., Zaidner, Y. & Yeshurun, R. A campsite on the open plain: Zooarchaeology of Unit III at the Middle Paleolithic site of Nesher Ramla, Israel. *Quaternary International* (2022) doi:10.1016/j.quaint.2020.01.026.

40. Garrod, D. A. & Bate, D. M. A. *The Stone Age of Mount Carmel. Volume 1: Excavations at the Wady El-Mughara*. (Clarendon Press, Oxford, 1937).

41. Munro, N. D. & Grosman, L. Early evidence (ca. 12,000 B.P.) for feasting at a burial cave in Israel. *PNAS* **107**, 15362–15366 (2010).

42. Yeshurun, R. & Bar-Oz, G. Digging in the Museum: Middle Paleolithic and Epipalaeolithic Faunal Remains from Olami's Prehistoric Survey of Mount Carmel. *Mitekufat Haeven: Journal of the Israel Prehistoric Society* **38**, 41–58 (2008).
43. Weinstein-Evron, M. *et al.* A Window into Early Middle Paleolithic human occupational layers: Misliya Cave, Mount Carmel, Israel. *Paleoanthropology* **2012**, 202–228 (2012).
44. Marín-Arroyo, A. B. New Opportunities for Previously Excavated Sites: Paleoeconomy as a Human Evolutionary Indicator at Tabun Cave (Israel). in *Zooarchaeology and Modern Human Origins: Human Hunting Behavior during the Later Pleistocene* (eds. Clark, J. L. & Speth, J. D.) 59–75 (Springer Netherlands, Dordrecht, 2013). doi:10.1007/978-94-007-6766-9_5.
45. Mercier, N. & Valladas, H. Reassessment of TL age estimates of burnt flints from the Paleolithic site of Tabun Cave, Israel. *Journal of Human Evolution* **45**, 401–409 (2003).
46. Mercier, N. *et al.* Hayonim Cave: a TL-based chronology for this Levantine Mousterian sequence. *Journal of Archaeological Science* **34**, 1064–1077 (2007).
47. Valladas, H. *et al.* Dating the Lower to Middle Paleolithic transition in the Levant: A view from Misliya Cave, Mount Carmel, Israel. *Journal of Human Evolution* **65**, 585–593 (2013).
48. Zaidner, Y. & Weinstein-Evron, M. The emergence of the Levallois technology in the Levant: A view from the Early Middle Paleolithic site of Misliya Cave, Israel. *Journal of Human Evolution* **144**, 102785 (2020).
49. Meignen, L. Contribution of Hayonim cave assemblages to the understanding of the so-called Early Levantine Mousterian. in *The Lower and Middle Paleolithic in the Middle East and neighbouring regions* (eds. Le et al.) vol. 126 85–100 (2011).
50. Meignen, L. Hayonim Cave Lithic Assemblages in the Context of the Near Eastern Middle Paleolithic. in *Neandertals and Modern Humans in Western Asia* (eds. Akazawa, T., Aoki, K. & Bar-Yosef, O.) 165–180 (Springer US, Boston, MA, 1998). doi:10.1007/0-306-47153-1_11.
51. Wojtczak, D. Hummal (Central Syria) and its eponymous industry. in *The Lower and Middle Palaeolithic in the Middle East and neighbouring regions.* (eds. Tensorer, J.-M. L., Jagher, R. & Otte, M.) 289–307 (Presses Universitaires de Liège, 2011).

52. Meignen, L. & Bar-Yosef, O. Acheulo-Yabrudian and Early Middle Paleolithic at Hayonim Cave (Western Galilee, Israel): Continuity or break? *Journal of Human Evolution* **139**, (2020).
53. Wojtczak, D. & Malinsky-Buller, A. The Levantine Early Middle Palaeolithic in retrospect – Reassessing the contribution of Abou-Sif to the understanding of Palaeolithic record. *Archaeological Research in Asia* **30**, 100366 (2022).
54. Shimelmitz, R. & Kuhn, S. Early Mousterian Levallois Technology in Unit IX of Tabun Cave. *PaleoAnthropology* 1–27 (2013).
55. Malinsky-Buller, A. The Muddle in the Middle Pleistocene: The Lower–Middle Paleolithic Transition from the Levantine Perspective. *J World Prehist* **29**, 1–78 (2016).
56. Hershkovitz, I. *et al.* The earliest modern humans outside Africa. *Science* **359**, 456–459 (2018).
57. Hovers, E. *The Lithic Assemblages of Qafzeh Cave*. (Oxford University Press, 2009).
58. Bar-Yosef, O. The Chronology of the Middle Paleolithic of the Levant. in *Neandertals and Modern Humans in Western Asia* (eds. Akazawa, T., Aoki, K. & Bar-Yosef, O.) 39–56 (Plenum Press, New York, 1998). doi:10.1007/0-306-47153-1_3.
59. Shea, J. J. The middle paleolithic of the east Mediterranean Levant. *Journal of World Prehistory* **17**, 313–394 (2003).
60. Groucutt, H. S., Scerri, E. M. L., Stringer, C. & Petraglia, M. D. Skhul lithic technology and the dispersal of Homo sapiens into Southwest Asia. *Quaternary International* (2017) doi:10.1016/j.quaint.2017.12.027.
61. Ekshtain, R. & Tryon, C. A. Lithic raw material acquisition and use by early Homo sapiens at Skhul, Israel. *J. Hum. Evol.* **127**, 149–170 (2019).
62. Fleisch, H. Les habitats du paléolithique moyen à Naamé (Liban). *Bulletin de la Musée de Beyrouth* **23**, 25–93 (1970).
63. Solecki, R. The Middle Paleolithic site of Nahr Ibrahim (Asfourieh Cave) in Lebanon. in *Problems in Prehistory: North Africa and the Levant, Southern Methodist University Press, Dallas, TX* (eds. Wendorf, F. & Marks, A. E.) 283–295 (Southern Methodist University Press, Dallas, 1975).
64. Copeland, L. *The Mousterian Site of Ras El-Kelb, Lebanon*. (BAR, 1998).

65. Zaidner, Y. *et al.* Middle Pleistocene Homo behavior and culture at 140,000 to 120,000 years ago and interactions with Homo sapiens. *Science* **372**, 1429–1433 (2021).

66. Prévost, M. & Zaidner, Y. New insights into early MIS 5 lithic technological behavior in the Levant: Nesher Ramla, Israel as a case study. *PLOS ONE* **15**, e0231109 (2020).

67. Centi, L. & Zaidner, Y. The Levallois Flaking System in Nesher Ramla Upper Sequence. *J Paleo Arch* **4**, 9 (2021).

68. Jelinek, A. J. The Middle Paleolithic in the Southern Levant with comments on the appearance of modern Homo sapiens. *The transition from Lower to Middle Palaeolithic and the origin of modern man* 57–104 (1982).

69. Jelinek, A. J. The Middle Paleolithic in the southern Levant from the perspective of the Tabun Cave. *Préhistoire du Levant* 265–280 (1981).

70. Vandermeersch, B. The first Homo sapiens sapiens in the Near East. in *The Transition from the Lower to the Middle Palaeolithic and the Origin of Modern Man* (ed. Ronen, A.) vol. 151 297–300 (BAR International Series, 1982).

71. McCown, T. D. & Keith, A. *The Stone Age of Mt. Carmel II, The Fossil Human Remains from the Levalloiso-Mousterian*. (Oxford, 1939).

72. Schwartz, J. H. & Tattersall, I. Fossil evidence for the origin of Homo sapiens. *Am J Phys Anthropol* **143**, 94–121 (2010).

73. Hershkovitz, I. *et al.* A new Middle Pleistocene Homo from Nesher Ramla, Israel. *Science* (2021).

74. Groucutt, H. S. *et al.* Homo sapiens in Arabia by 85,000 years ago. *Nature Ecology & Evolution* **2**, 800 (2018).

75. Scerri, E. M. L. *et al.* Middle to Late Pleistocene human habitation in the western Nefud Desert, Saudi Arabia. *Quaternary International* **382**, 200–214 (2014).

76. Crassard, R. *et al.* Middle Palaeolithic and Neolithic Occupations around Mundafan Palaeolake, Saudi Arabia: Implications for Climate Change and Human Dispersals. *PLOS ONE* **8**, e69665 (2013).

77. Groucutt, H. S. *et al.* Rethinking the dispersal of Homo sapiens out of Africa. *Evol. Anthropol.* **24**, 149–164 (2015).

78. Petraglia, M. D. *et al.* Hominin Dispersal into the Nefud Desert and Middle Palaeolithic Settlement along the Jubbah Palaeolake, Northern Arabia. *PLOS ONE* **7**, e49840 (2012).
79. Richter, D., LeTensorer, J.-M., Hauck, T. C., Wojtczak, D. & Muhesen, S. Chronometric age estimates for the site of Hummal (El Kowm, Syria). in *The Lower and Middle Palaeolithic in the Middle East Neighbouring Regions* (eds. Le Tensorer, Jagher, R. & Otte, M.) 249–261 (Presses Universitaires de Liège, Liège, 2011).
80. Schwarcz, H. P. *et al.* ESR dates for the hominid burial site of Qafzeh in Israel. *Journal of Human Evolution* **17**, 733–737 (1988).
81. Grün, R. *et al.* U-series and ESR analyses of bones and teeth relating to the human burials from Skhul. *J. Hum. Evol.* **49**, 316–334 (2005).
82. Grün, R. & Stringer, C. Tabun revisited: revised ESR chronology and new ESR and U-series analyses of dental material from Tabun C1. *J. Hum. Evol.* **39**, 601–612 (2000).
83. Porat, N. & Schwarcz, H. P. Use of signal subtraction methods in ESR dating of burned flint. *International Journal of Radiation Applications and Instrumentation. Part D. Nuclear Tracks and Radiation Measurements* **18**, 203–212 (1991).
84. Zaidner, Y. *et al.* A series of Mousterian occupations in a new type of site: The Nesher Ramla karst depression, Israel. *Journal of Human Evolution* **66**, 1–17 (2014).
85. Copeland, L. The Middle and Upper Palaeolithic of Lebanon and Syria in the light of recent research. in *Problems in prehistory: North Africa and the Levant* (eds. Wendorf, F. & Marks, A. E.) 317–350 (Southern Methodist University Press, Dallas, 1975).
86. Groucutt, H. S. *et al.* Human occupation of the Arabian Empty Quarter during MIS 5: evidence from Mundafan Al-Buhayrah, Saudi Arabia. *Quaternary Science Reviews* **119**, 116–135 (2015).
87. Groucutt, H. S. *et al.* Late Pleistocene lakeshore settlement in northern Arabia: Middle Palaeolithic technology from Jebel Katefeh, Jubbah. *Quaternary International* **382**, 215–236 (2015).
88. Prévost, M., Centi, L. & Zaidner, Y. The use of the lateral tranchet blow technique at Nesher Ramla (Israel): a new cultural marker in the Levantine Middle Paleolithic? *Quaternary International* (2022) doi:10.1016/j.quaint.2020.11.008.

89. Zaidner, Y. & Grosman, L. Middle Paleolithic sidescrapers were resharped or recycled? A view from Nesher Ramla, Israel. *Quaternary International* **361**, 178–187 (2015).

90. Meignen, L. The Mousterian lithic assemblages from Kebara Cave. in *Kebara Cave, Mt. Carmel, Israel: The Middle and Upper Paleolithic Archaeology. Part II* (eds. Meignen, L. & Bar-Yosef, O.) 1–149 (American School of Prehistoric Research Bulletin 51, Harvard University, Peabody Museum of Archaeology and Ethnology, Cambridge, 2019).

91. Hovers, E. The lithic assemblages of Amud Cave: implications for the end of the Mousterian in the Levant. in *Neandertals and Modern Humans in Western Asia* (eds. Akazawa, T., Aoki, K. & Bar-Yosef, O.) 143–163 (Plenum Press, New York Plenum, 1998).

92. Groucutt, H. S. Middle Palaeolithic point technology, with a focus on the site of Tor Faraj (Jordan, MIS 3). *Quaternary International* **350**, 205–226 (2014).

93. Pagli, M. Middle Palaeolithic variability in the Near East as a reflection of different settlement dynamics: A comparative study of Umm el Tlel, Yabroud I (Syria) and Ksar'Akil (Lebanon). in *Settlement Dynamics of the Middle Paléolithic and Middle Stone Age, Volume IV* (eds. Conard, N. J. & Delagnes, A.) (Kerns Verlag, Tübingen Publications in Prehistory, 2015).

94. Barzilai, O. *et al.* Rediscovering Geula Cave: A Middle Paleolithic cave site in northern Mt. Carmel, Israel. *Quaternary International* (2021) doi:10.1016/j.quaint.2021.03.007.

95. Wojtczak, D. The Early Middle Palaeolithic Blade Industry from Hummal, Central Syria. (University of Basel, Basel, 2014).

96. d'Errico, F., Salomon, H., Vignaud, C. & Stringer, C. Pigments from the Middle Palaeolithic levels of Es-Skhul (Mount Carmel, Israel). *Journal of Archaeological Science* **37**, 3099–3110 (2010).

97. Bar-Yosef Mayer, D. E., Vandermeersch, B. & Bar-Yosef, O. Shells and ochre in Middle Paleolithic Qafzeh Cave, Israel: indications for modern behavior. *Journal of Human Evolution* **56**, 307–314 (2009).

98. Godfrey-Smith, D. I. & Ilani, S. Past thermal history of goethite and hematite fragments from Qafzeh Cave deduced from thermal activation characteristics of the 110°C TL peak of enclosed quartz grains. *ArchéoSciences, revue d'Archéométrie* **28**, 185–190 (2004).

99. Solecki, R. A Ritual Middle Palaeolithic Deer Burial at Nahr Ibrahim Cave, Lebanon. *MOM Éditions* **12**, 47–56 (1982).

100. Tsatskin, A. & Zaidner, Y. Geoarchaeological context of the later phases of Mousterian occupation (80–115 ka) at Nesher Ramla, Israel: Soil erosion, deposition and pedogenic processes. *Quaternary International* **331**, 103–114 (2014).

101. Vandermeersch, B. & Bar-Yosef, O. The Paleolithic Burials at Qafzeh Cave, Israel. *PALEO. Revue d'archéologie préhistorique* 256–275 (2019) doi:10.4000/paleo.4848.

102. Yeshurun, R., Malkinson, D., Crater Gershtein, K. M., Zaidner, Y. & Weinstein-Evron, M. Site occupation dynamics of early modern humans at Misliya Cave (Mount Carmel, Israel): Evidence from the spatial taphonomy of faunal remains. *Journal of Human Evolution* **143**, 102797 (2020).

103. Stiner, M. C. *The Faunas of Hayonim Cave, Israel: A 200,000-Year Record of Paleolithic Diet, Demography, and Society*. (Harvard University Press, 2005).

104. Speth, J. D. Kebara as a Late Pleistocene Settlement. Insights from the Ungulate Remains). in *Kebara Cave, Mt. Carmel, Israel. The Middle and Upper Paleolithic Archaeology. Part II* (eds. Meignen, L. & Bar-Yosef, O.) (Harvard University, Peabody Museum of Archaeology and Ethnology, Cambridge, 2019).

105. Rabinovich, R. & Hovers, E. Faunal analysis from Amud Cave: preliminary results and interpretations. *International Journal of Osteoarchaeology* **14**, 287–306 (2004).

106. Malinsky-Buller, A., Ekshtain, R., Munro, N. & Hovers, E. Back to base: re-thinking variations in settlement and mobility behaviors in the Levantine Late Middle Paleolithic as seen from Shovakh Cave. *Archaeol Anthropol Sci* **13**, 112 (2021).

107. Rabinovich, R., Bar-Yosef, O., Vandermeersch, B. & Horwitz, L. Hominid-carnivore interactions in the Paleolithic site of Qafzeh cave, Israel. *Revue de Paleobiologie* **23**, 627–637 (2004).